

Review

Recent Progress in Light-Triggered Nanotheranostics for Cancer Treatment

Pengcheng Zhang^{1*}, Chunhua Hu^{1,2*}, Wei Ran^{1,3}, Jia Meng^{1,3}, Qi Yin¹, Yaping Li¹✉

1. State Key Laboratory of Drug Research & Center for Pharmaceutics, Shanghai Institute of Materia Medica, Chinese Academy of Sciences, Shanghai 201203, China;
2. Nano Science and Technology Institute, University of Science and Technology of China, Suzhou 215123, China;
3. University of Chinese Academy of Sciences (UCAS), Beijing 100049, China.

*The two authors contributed equally to this work.

✉ Corresponding author: Prof. Yaping Li, State Key Laboratory of Drug Research & Center for Pharmaceutics, Shanghai Institute of Materia Medica, Chinese Academy of Sciences, 501 Haike Road, Shanghai 201203, China. Phone/Fax: +86-21-20231979; Email: ypli@simm.ac.cn.

© Ivyspring International Publisher. Reproduction is permitted for personal, noncommercial use, provided that the article is in whole, unmodified, and properly cited. See <http://ivyspring.com/terms> for terms and conditions.

Received: 2016.02.07; Accepted: 2016.03.24; Published: 2016.04.27

Abstract

Treatments of high specificity are desirable for cancer therapy. Light-triggered nanotheranostics (LTN) mediated cancer therapy could be one such treatment, as they make it possible to visualize and treat the tumor specifically in a light-controlled manner with a single injection. Because of their great potential in cancer therapy, many novel and powerful LTNs have been developed, and are mainly prepared from photosensitizers (PSs) ranging from small organic dyes such as porphyrin- and cyanine-based dyes, semiconducting polymers, to inorganic nanomaterials such as gold nanoparticles, transition metal chalcogenides, carbon nanotubes and graphene. Using LTNs and localized irradiation in combination, complete tumor ablation could be achieved in tumor-bearing animal models without causing significant toxicity. Given their great advances and promising future, we herein review LTNs that have been tested *in vivo* with a highlight on progress that has been made in the past a couple of years. The current challenges faced by these LTNs are also briefly discussed.

Key words: Nanoparticle, theranostics, imaging, photodynamic, photothermal.

Introduction

Cancer is among the leading causes of death in the world, with 14.1 million incidences and 8.2 million deaths estimated in 2012 [1]. Efforts in both fundamental research and clinical practices revealed that cancer is a systemic disease involving both cancerous and normal cells, and single modality treatments are far from efficient to eradicate primary and metastasized tumors of high heterogeneity [2]. Therefore, the combination use of surgery, radiotherapy, chemotherapy and immunotherapy is routine in the clinic. Discouragingly, the response rate is low and the duration of effect is transient, largely due to the heterogeneity among patients and the ability of cancer cells to adapt and survive treatment [2, 3]. More importantly, severe side effects occur even if the treatment is of less or no effect. Thus, it is of critical importance to optimize treatment for

individual patients to achieve the highest therapeutic efficiency along with the best safety profile. Theranostic agents that are able to detect tumors and their pathology, predict and monitor the response to treatment, and exert specific and controlled therapy is highly desirable to achieve this goal.

Since one theranostic agent is expected to exert multiple functions, modalities with different functions must be integrated into one entity, which is challenging from a molecular design and synthesis perspective. This issue could be addressed with nanotechnology, obtaining nanotheranostics that are predominantly nano-sized theranostic agents with three “faces” (Figure 1) [4, 5]. Firstly, the nanotheranostics are nano-sized objects, and thus possess the common capabilities of nano-objects such as preferential accumulation in the tumor through the

enhanced permeation and retention (EPR) effect, feasible surface modification, and multifunctionality. Secondly, the nanotheranostics are imaging agents able to detect and diagnose the disease, and monitor its response to the applied treatment. Finally, nanotheranostics are therapeutic agents capable of treating tumors via different mechanisms of action. The use of nanotheranostics improves the specificity of the treatment, and allows the accumulation and effect of the drug to be monitored in real time, helping to assess the potential benefit and risk of treatment before extensive dosing. Due to the obvious advantages of nanotheranostics [6, 7], much effort has been devoted to design and develop new and powerful nanotheranostics over the past few years.

Light-triggered nanotheranostics (LTN) are entities that can be remotely triggered to exert anti-tumor activity through light irradiation (Figure 1), and have therefore attracted extra attention from researchers, mainly for the following reasons: (1) optical imaging techniques have already been widely used in both clinic and laboratory for tumor imaging and biomolecule detection [8, 9]; (2) many photosensitizers (some of which are in clinical use) have been reported to kill the cancer cells by generating local hyperthermia, reactive oxygen species (ROS) or singlet oxygen (1O_2), with no significant resistance to the treatment observed so far [10]; (3) multiple light-triggered functions could be easily integrated into one single particle in a well-defined pattern through elegant but feasible construction techniques [10]; and (4) compared with

other activation modalities used in nanotheranostics construction, near-infrared light (NIR) has several obvious advantages such as low treatment invasiveness, rare non-specific activation, high spatiotemporal precision, real-time dosage adjustment and the capability to be switched on and off. Given their potential in cancer treatment, this review will focus mainly on LTNs, particularly on their progress in the past two years. The following sections start with a brief introduction on the mechanism of light-triggered therapeutics, followed by a discussion on LTNs constructed from different photosensitizers (PSs). The current challenges of LTNs are also discussed.

Light-triggered therapy and imaging

Triggering a biological effect with light is not a new phenomenon, having been widely adopted by almost all living organisms. For instance, chlorophyll, a class of specialized chromophores, captures energy from light to generate high energy chemical intermediates, and the energy is then transferred, stored, utilized, and dissipated. The PS, such as chlorophyll, is the key component for all light-activated systems including LTNs. Many PSs have so far been discovered and synthesized [11, 12], including nanomaterials with unique photo properties [13-15], which enables the construction of a wide variety of LTNs. The way they respond to light irradiation accordingly depends on the chemical property of the incorporated PS.

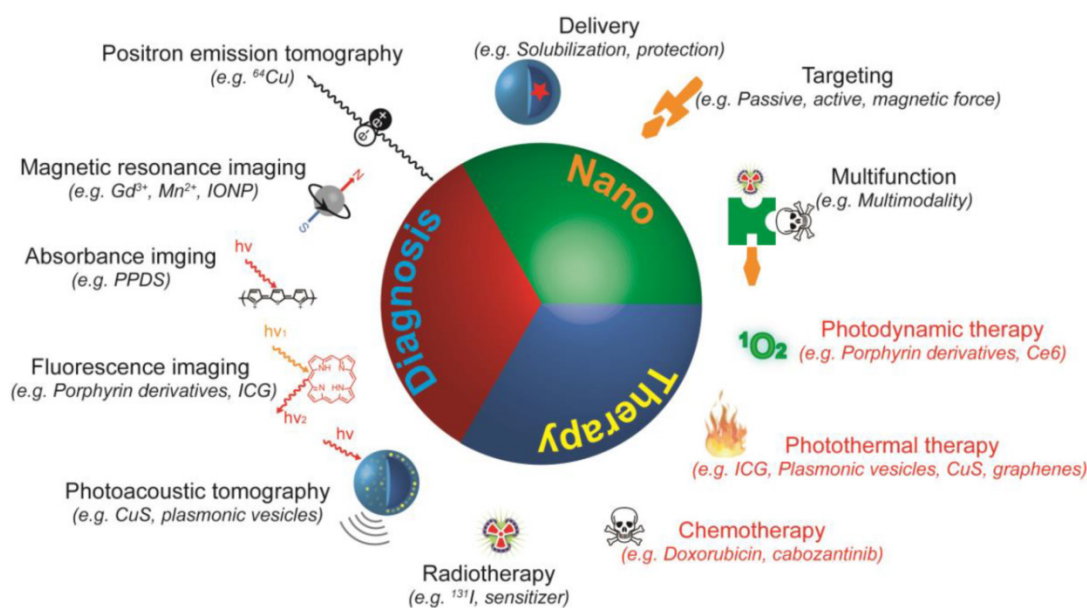


Figure 1. Schematic illustration of nanotheranostics. A nanotheranostic agent is a single entity with three characteristics: nano-sized particle, therapeutic agent, and diagnostic agent. As nano-sized particles, nanotheranostics help to solubilize and protect cargos, improve accumulation of both contrast and therapeutic agents at the disease site, and enable integration of multiple functions into one single particle. As therapeutic agents, nanotheranostics can eradicate cancer cells via singlet oxygen (1O_2) or ROS generation, hyperthermia, radiation, or the release of chemotherapeutics. As diagnostic agents, nanotheranostics provide contrast for positron emission tomography (PET), magnetic resonance imaging (MRI), absorbance imaging, fluorescence imaging, or photoacoustic tomography. Nanotheranostics that exert a therapeutic effect upon light irradiation (red) were termed as light-triggered nanotheranostics or LTNs, which are the focus of this review.

Organic dyes and carbons-based materials closely resemble chlorophyll in their response to light irradiation. The absorption of a photon by these PSs would elevate an electron of the PS from its ground state to a higher excited state, and the molecule is then placed in the lowest vibrational level of the excited state through internal relaxation. The further relaxation of the molecule could then result in: (1) the emission of a photon with a Stokes shift in wavelength; (2) the transfer of energy to its surrounding environment as heat; or (3) conversion from singlet to triplet state, followed by photon emission or generation of ROS (type I) or $^1\text{O}_2$ (type II) [16, 17]. During the light-triggered therapy of cancer, heat and $^1\text{O}_2$ are the two major effectors. Heat generated by the PS could cause hyperthermia of the irradiated tissues, denoted as photothermal therapy (PTT). Raising the temperature of the tumor to 42 °C can make the cancer cells more susceptible to additional treatments such as irradiation and chemotherapy, in addition to causing a degree of apoptosis. Direct cell death can also be induced in the tumor by raising the temperature of tumor to 45 °C or above [18]. $^1\text{O}_2$ kills the cancer cells through the destruction of important biomolecules and membrane enveloped structures, a treatment termed photodynamic therapy (PDT). Since the lifespan of $^1\text{O}_2$ is less than 3.5 microseconds and it can diffuse only 10 to 20 nm [19], $^1\text{O}_2$ can only exert damage within a limited distance, resulting in local cell death by apoptosis, necrosis, or autophagy [20]. Aside from the two therapeutic effectors, the fluorescence, photoacoustic (PA) signal and the surface enhanced Raman scattering (SERS) of LTNs upon light irradiation could be used for tumor imaging in living objects [21, 22].

The response of metal-based nanomaterials to light irradiation is quite different to that of organic PSs. Light incident on noble metal [23] or semiconductor [24, 25] nanoparticles induces the oscillation of conduction electrons relative to the lattice of positive ions with a frequency that depends on the properties of nanoparticles (e.g. size, shape and composition) and their environment, a phenomenon known as localized surface plasmon resonance (LSPR). The strong surface plasmon oscillation then decays either nonradiatively as heat or by radiating its energy as light [23, 26], allowing the application of these inorganic nanoparticles in PTT, PA and optical imaging of tumors [27]. LSPR could also exponentially enhance the Raman scattering of molecules in the vicinity of the nanostructures, and thus enable SERS-based imaging of cancer [23]. There are also other mechanisms through which inorganic nano-sized PSs interact with photons. For instance,

some metal oxides (TiO_2 and ZnO), while being irradiated with UV light, are able to form photo-induced hole–electron pairs that can interact with surrounding O_2 and H_2O to generate reactive oxygen species (ROS) for PDT [28, 29].

Light-triggered cancer therapy through other mechanisms, such as photoisomerization and photocleavage-induced drug activation and release, has also been reported [30, 31]. For instance, light-triggered drug (doxorubicin or gentamicin) release from liposomes was achieved with precise spatial and temporal control by incorporating 2% or 10% (molar ratio) porphyrin–phospholipid into liposomes and irradiating the tumor with a laser [32, 33]. Nevertheless, few LTNs based on these mechanisms have been developed [34]. The following part of this review will mainly discuss the most recent progress in LTNs constructed from small molecular and polymeric organic PSs, nanocrystals or carbon-based nano-objects, which eradicate cancer cells through PDT and PTT.

Organic LTNs

Phototherapy of cancers using organic PSs have a history dating back to 1975, when Dougherty and colleagues reported that hematoporphyrin administration followed with light irradiation could cure animal tumors [35]. Many organic PSs have since been developed, some of which are already in clinical use for the treatment of superficial cancers [13, 36]. Despite their light-controlled efficacy and biocompatibility, most small molecular PSs suffer from poor pharmacokinetic properties. Thus, these PSs were made into LTNs, generally via two strategies [26, 36–39]: self-assembly of a small molecule PS into an LTN and using functional nanoparticles to deliver these PSs (Figure 2). In addition, the imaging potential of PSs could also be improved when they were made into LTNs. Currently, the most investigated organic PSs are porphyrin-, cyanine-, and polymer-based dyes, which will be discussed below in detail.

Porphyrin-based LTNs

Porphyrin-based photosensitizers are a class of heterocyclic aromatic ring containing small molecules (such as porphyrin, chlorin and bacteriochlorin) that can emit fluorescence and generate $^1\text{O}_2$ or heat upon light irradiation. A number of porphyrin-based PSs have been approved by the Food and Drug Administration (FDA) for clinical use [40], however their application is limited by poor aqueous solubility, low cancer specificity, and low sensitivity in cancer imaging.

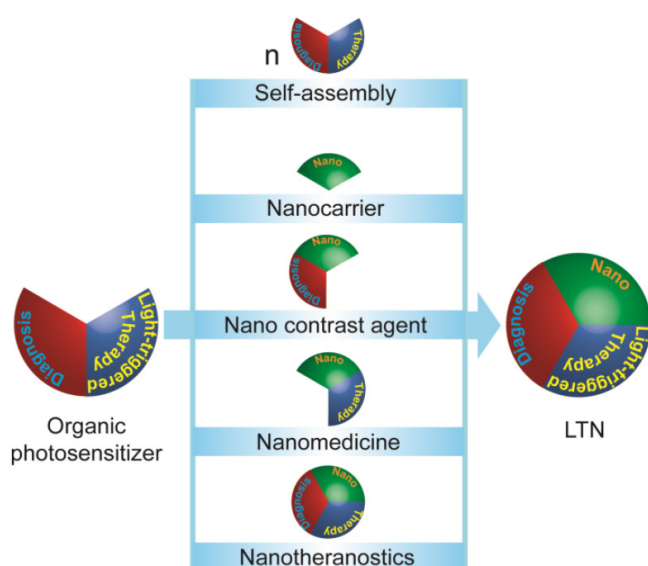


Figure 2. Strategies for constructing light-triggered LTN from small molecular organic photosensitizers (PSs). Small molecular PSs which provide contrast for imaging and a therapeutic effect upon irradiation could be built into LTNs via five strategies: (1) the small molecular PS could be modified and induced to self-assemble into discrete LTNs; (2) nanocarriers, (3) nano-sized contrast agents, (4) nanomedicine, or even (5) LTNs could be used as transporter for small molecular PSs.

Assembling porphyrin-based PSs into nanostructures is a feasible and widely adopted way to improve their pharmacokinetic properties, taking advantage of the hydrophobic collapse and π - π stacking between porphyrin-based PSs. For instance, Zheng and colleagues constructed a porphosome (a liposome-like vesicle) by co-assembling pyropheophorbide-phospholipid conjugates with PEGylated phospholipid (19:1, mol/mol) [41]. The close packing of pyropheophorbide in the bilayer of porphosomes facilitated the conversion of light into heat rather than fluorescence and $^1\text{O}_2$ generation. Their extensive intratumoral accumulation was confirmed with PA tomography and porphosome destruction-activated fluorescence imaging. Subcutaneous xenograft tumors in mouse models were completely eradicated through PTT after intravenous injection of porphosome at 42 mg/kg followed with local 680 nm laser irradiation (1.9 W/cm², 1 min) 24 h after injection. Recently, the PTT efficacy of porphosomes has been successfully confirmed using rabbit and hamster models bearing hand and neck cancers [42]. Intriguingly, the porphosomes could also be turned into PDT agents with near 100% $^1\text{O}_2$ generation efficiency through simple palladium chelation, and into a SERS contrast agent for tumor imaging [22]. Triple-modality imaging (ultrasound, photoacoustic and fluorescence) could be realized by encapsulating a perfluorocarbon gas into bacteriochlorophyll-lipid microbubbles, a porphosome-like vesicle that transforms into nanobubbles under ultrasound [43]. These findings

suggest that vesicles assembled from porphyrin-based PSs could be a versatile LTN for PDT/PTT based tumor ablation and multi-modality tumor imaging. Other than a covalent conjugation strategy, porphyrin-based PSs could also be introduced into vesicles non-covalently. Recently, a benzoporphyrin derivative (BPD) was physically loaded into the lipid bilayer of nanoliposomes for PDT applications, providing a fluorescence imaging capability and controlled release of encapsulated cabozantinib (a multikinase inhibitor) (Figure 3A) [44]. PDT here triggered the apoptosis of cancer cells and endothelial cells, while cabozantinib suppressed the anti-apoptosis and VEGF signaling, achieving a significant synergistic effect. More importantly, cabozantinib also inhibited MET—the receptor tyrosine kinase for hepatocyte growth factor—signaling to suppress cancer cell motility and invasion, and thus prevented metastatic escape of cancer.

Other than vesicles, porphyrin-based PSs could also be engineered into micelle-like particles by conjugating the PS with biopolymers such as peptides, polysaccharides and their derivatives [45-48]; into solid particles via loading of porphyrin-based PS into nanoparticles [49, 50]; or into bio-mimicking particles through mixing of porphyrin-based PS derivatives with functional peptides [51]. Bio-responsive or bio-mimicking LTNs incorporating porphyrin-based PS are the current focus of this area, as high tumor specificity and biocompatibility could be achieved. Tumor microenvironment-responsive LTNs were prepared by conjugating the porphyrin-based PS, Purpurin18, to a matrix metalloproteinase (MMP) sensitive (in bold) and integrin targeting (underlined sequence) peptide, **PLGVRGRGD** (Pro-Leu-Gly-Val-Arg-Gly-Arg-Gly-Asp) [45]. The obtained conjugates were water soluble with preferential accumulation in the tumor, wherein they were cleaved by MMP and self-assembled into nanofibers. PA tomography revealed improved accumulation and prolonged retention of Purpurin18 in the tumor, and complete tumor ablation via PTT was observed after laser irradiation (at 6 and 10 h after intravenous injection of ~60 μg of the conjugate, 730 nm, 1.2 W/cm², 5 min). In addition to this strategy, nanoparticles that could mimic long circulating bio-particles in the blood were developed for the purpose of enhancing tumor accumulation, taking advantage of the EPR effect. For instance, high density lipoprotein (HDL) is a spherical nanoparticle (8-12 nm) circulating in blood for cholesterol transportation, and has great potential for drug delivery [52]. Recently, a HDL particle-mimicking porphylipoprotein (PLP) was

constructed, comprising ^{64}Cu -porphyrin-lipid conjugate, cholesteryl oleate, 1,2-dimyristoyl-*sn*-glycero-3-phosphocholine (DMPC), ApoA-1 mimetic R4F peptide, Ac-FAEKFKYAKVDFAKFWD, and 1,10-Dioctadecyl-3,3,30,30-tetramethylindotricarbocyanine iodide bis-oleate (DiR-BOA) (Figure 3B) [51]. The PLP had a long half-life of 9.9 h with improved fluorescence and photodynamic activation when compared to porphyrin, possibly due to the weaker intermolecular packing. The PLP successfully detected intracranial grafted glioblastoma, orthotopic prostate cancer, and ovarian cancer metastases via integrated fluorescence molecular tomography and computed tomography (FMT/CT) and integrated positron emission tomography and computed tomography (PET/CT) imaging, taking advantage of the fluorescence from porphyrin and DiR-BOA, and the PET signal from ^{64}Cu -porphyrin.

In addition to the self-assembly strategy that was applied to construct porphyrin-based LTNs, functional inorganic nano-objects have also been used as carriers. These functional inorganic nanoparticles both improve the delivery of porphyrin-based PSs and allow for multi-modality tumor imaging. Graphene, a carbon-based two-dimensional

honeycomb lattice [53], has proven to be an efficient carrier for porphyrin-based PSs, likely due to the strong associative π - π interaction between the PS and graphene [54]. In this case sinoporphyrin sodium, a porphyrin dimer salt with two sterically hindered porphyrin rings, was used instead of its monomer to prevent fluorescence quenching. Carbon dots, another type of carbon-based nanoparticle, have also been used as carriers for zinc phthalocyanine (ZnPc) to achieve simultaneous imaging and targeted PDT [55]. Nano-sized contrast agents have been used as carrier for PSs to build LTNs that can perform multi-modality imaging. Silica-coated gold nanoclusters (AuNCs@SiO₂) are one of these nano-sized contrast agents [56]. AuNCs are subnanometer particles consisting of several to tens of gold atoms. The spatial confinement of free electrons in AuNCs could lead to molecular-like properties such as luminescence, and thus could be used as a fluorescence imaging contrast agent [57]. While silica-coatings are widely used to stabilize AuNCs, they can also provide a framework for further functionalization, with the Chlorin e6 (Ce6) PS in this instance. Fluorescence imaging-guided PDT was successfully performed using a combination of

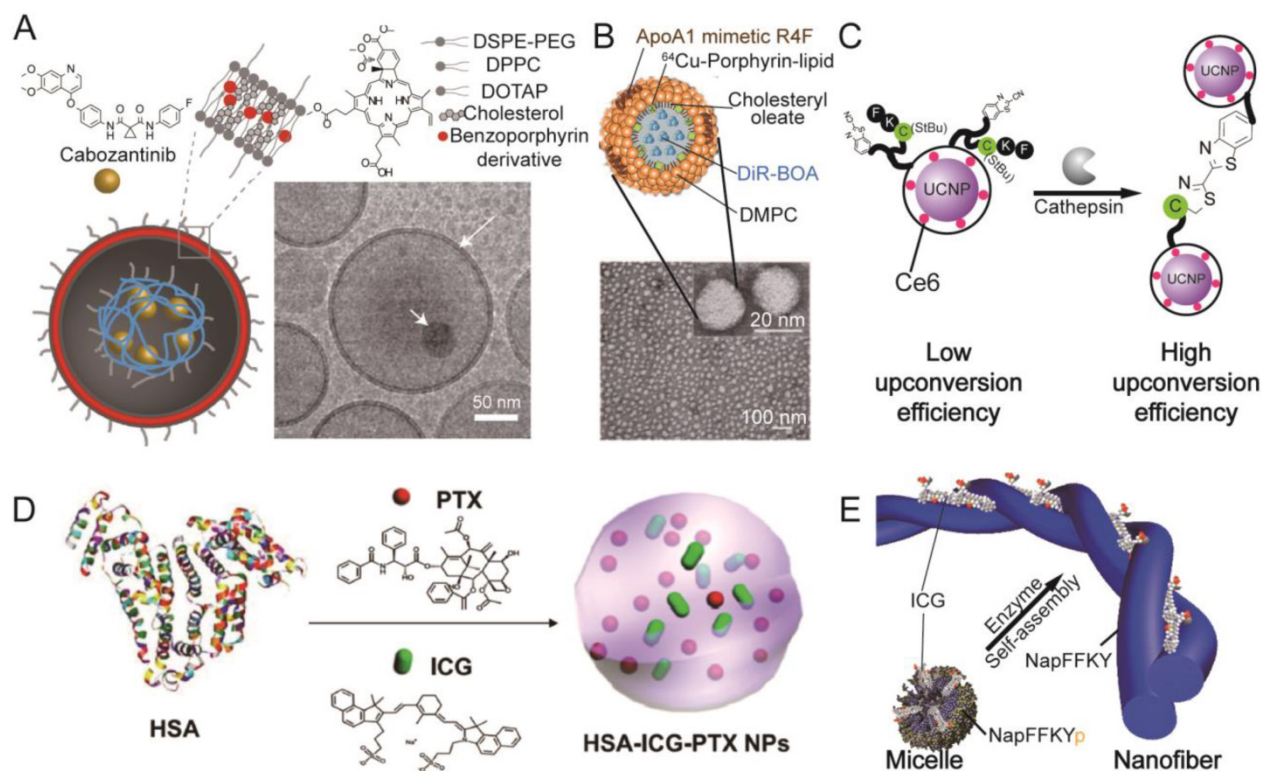


Figure 3. Representative organic photosensitizer-based LTNs. (A) Schematic illustration and cryo-TEM imaging of the photoactivable multi-inhibitor nanoliposome. The nanoliposome bilayer was composed of DSPE-PEG, DPPC, DOTAP, cholesterol, and a benzoporphyrin derivative that could be activated by light. The cabozantinib encapsulated in the hollow cavity could be released upon light irradiation. Adapted with permission from [44]. (B) Schematic illustration and TEM imaging of a HDL mimetic nanotheranostic which is highly stable in circulation. Adapted with permission from [51]. (C) Schematic illustration of a tumor microenvironment sensitive LTN which would aggregate in the tumor, resulting in improved fluorescence emission for Ce6 activation. Adapted with permission from [67]. (D) The preparation of an “Abraxane-like” nanotheranostic from HAS, PTX and ICG. Adapted with permission from [82]. (E) Schematic illustration of a tumor microenvironment sensitive ICG-loaded LTN that could undergo a morphological transition from micelle to nanofiber. Adapted with permission from [77].

AuNCs@SiO₂-Ce6 and 671 nm laser irradiation (0.1 W/cm², 10 min). Iron oxide nanoclusters (IONCs) are another nano-sized contrast agents that were explored as carriers for Ce6, and the resulting LTN enables dual-modality imaging (magnetic resonance imaging (MRI) and fluorescence imaging) and PDT of the tumor [58, 59]. More importantly, this LTN could be guided to accumulate in the tumor through use of an external magnetic field to achieve efficient PDT. When a pH-sensitive polymer-Ce6 conjugate was used in the preparation of iron oxide nanoclusters (named as magnetic nanogrenades), the MRI, fluorescence imaging and PDT activity of the formed LTN could be specifically turned on in the acidic tumor microenvironment, contributing to the specificity of tumor imaging and treatment [60].

Functional inorganic nanoparticles can not only aid in tumor targeted imaging and PS delivery, but also enhance the photo-¹O₂ conversion efficiency of porphyrin-based PSs. One such example is upconversion nanoparticles (UCNPs) that exhibit anti-Stokes behavior due to double energy transfer from Yb³⁺ to Er³⁺ upon irradiation and the emission of a single photon by excited Er³⁺ [61]. Taking advantage of the anti-Stokes behavior of UCNPs, near infra-red (NIR) lasers (deep tissue penetration) could be used to activate the carried PS, whose optimal excitation wavelength lies in the visible range, through fluorescence resonance energy transfer (FRET) from the UCNPs to the PSs. The potential of NaYF₄:Yb,Er/PS core-shell nanoparticles in PDT has been proven both *in vitro* and *in vivo* [62-66]. For instance, a surface-modified UCNP that could accumulate and aggregate in the tumor in response to tumor-specific cathepsin has been used as carrier for Ce6 to construct LTNs. Compared with conventional UCNPs, the modified UCNP after aggregation showed improved upconversion efficiency, resulting in improved fluorescence emission, Ce6 excitation, and ¹O₂ generation for tumor imaging and therapy (Figure 3C) [67]. More importantly, it is feasible to integrate additional functional modalities into the core-shell structured LTN. For example, MRI modality could be incorporated into the LTN by doping gadolinium (Gd) into the UCNP [68, 69], and chemotherapeutics could be carried together with PS by a single UCNP to achieve a synergistic effect [69, 70]. In these cases, the tumor was highlighted by the accumulated LTNs through MRI and/or fluorescence imaging, and localized irradiation with 980 nm laser instead of short wavelength laser (e.g. 671 nm laser) led to efficient PDT as evidenced by tumor regression. In addition to UCNPs, carbon dots have also been used as FRET donors for Ce6, and efficient tumor detection and ablation was reported [71].

Porphyrin-based PSs have been used for the phototherapy of cancer for many years, with much success in the treatment of superficial tumors. However, their further application is limited by their poor solubility, low specificity, and poor sensitivity. Many porphyrin-based LTNs were recently developed and tested *in vivo*, and promising results were achieved from the aspects of both tumor imaging and therapy. The imaging-guided tumor therapy greatly improved the specificity of the treatment, realizing complete tumor ablation without significant side effects. Synergistic effects could be achieved when multiple therapeutic modalities were rationally combined, as exemplified by the work reported by Hasan and colleagues [44]. Nevertheless, the long-term toxicity of porphyrin-based LTNs needs to be fully assessed, which is critical for their clinical application as many porphyrin-based PSs exhibit phototoxicity, especially when accumulated in the skin [72].

Cyanine-based LTNs

Porphyrin-based PSs typically exert their light-triggered anticancer activity via PDT, a process requiring the presence of oxygen in the environment. However, many solid tumors possess cores that are oxygen-deficient (hypoxic) [73], greatly limiting ¹O₂ generation and thus the efficacy of PDT. Organic PSs that eradicate cancer cells through PTT are an alternative choice, and cyanine-based dyes are among the most investigated. Cyanines are a class of synthetic dyes characterized by the polymethine functional group, and have been broadly used in fluorescence-based imaging. Indocyanine green (ICG), for example, has been in clinical use as a blood flow imaging agent for more than 50 years, due to its maximum absorption at approximately 800 nm and emission at around 830 nm [32]. However, the quantum yield of ICG is low and a large portion of the absorbed energy is dissipated as heat, a property that favors the application of ICG as a photothermal agent. In addition, free ICG suffers from poor solubility and photostability, high plasma protein binding rate, rapid clearance from the body (2-4 min), and low cancer selectivity [74]. Nanoparticle-based ICG has been proven to be a feasible way to address these issues and realize simultaneous tumor imaging and PTT.

Many nano-sized carriers, including polymeric complexes [75, 76], peptides [77], proteins [78-84], micelles [85-88], vesicles [89], UCNPs [90], or magnetic particles [91] have been used to develop ICG-based LTNs. Among those carriers, bio-derived nanoparticles such as human serum albumin (HSA) have received much attention because of their

superior biocompatibility. HSA is a 66.5 kDa serum protein with a half-life of ~20 days in circulation. It contains at least two hydrophobic domains, many primary amine groups and carboxyl groups, and one free thiol (Cys 34) [92], allowing both non-covalent PS binding and covalent PS conjugation. For example, CySCOOH, a carboxyl group containing derivative of ICG, could be conjugated to HSA through an amide bond [83]. Improved tumor accumulation and retention was observed by fluorescence and PA imaging when compared with free CySCOOH, and complete tumor photothermal ablation was achieved when combined with localized laser irradiation (808 nm, 1 W/cm², 5 min). MRI contrast agents could be introduced onto PS-loaded HSA using a similar method, allowing for simultaneous MRI, fluorescence imaging, and PTT [80]. Due to the success of albumin nanoparticles in drug delivery [93], cross-linked HSA nanoparticles 75 nm in diameter (by DLS) have been explored as a carrier for ICG [78]. The half-life of ICG-loaded HSA nanoparticle was 2.86 h in high contrast to 0.12 h of free ICG. The accumulation of intravenously injected LTN in a subcutaneous xenograft 4T1 tumor could be clearly visualized via fluorescence and PA imaging. After imaging-guided precise tumor irradiation with an 808 nm laser (0.8 W/cm², 5 min), complete tumor regression was observed due to the PDT and PTT from ICG with no tumor recurrence and related toxicity observed. Liu and colleagues went one step further and constructed a photothermal "Abraxane-like" LTN by inducing the co-assembly of HSA, paclitaxel (PTX) and ICG (Figure 3D) [82]. The formed HSA-ICG-PTX complexes were 80 nm in diameter, and showed preferential accumulation in the primary and lung metastasized tumors as evidenced by fluorescence imaging. More importantly, both primary and metastasized tumors were successfully treated through the combination of chemotherapy and imaging-guided PTT. In addition to HSA, ferritin, a natural protein for iron storage and metabolism [94], has also been explored as a carrier for the NIR dye IR820 [81]. The intriguing part of the design is that the ferritin could undergo disassembly and re-assembly in response to changes in pH, a process during which cargos could be loaded into its hollow cavity. Taking advantage of its small size, high loading rates and biocompatibility, significant tumor accumulation was observed via fluorescence and PA imaging, and PTT-mediated tumor ablation was achieved when irradiating the tumor with an 808 nm laser (0.5 W/cm², 10 min).

Compared with conventional nanocarriers, stimuli-responsive nanocarriers possess additional features such as controlled tissue accumulation and drug release [30]. It has been demonstrated that

cypate-containing micelles that disassembled at tumor-relevant pH improved the therapeutic outcome of drug resistant cancer [95]. Chen and colleagues successfully improved the tumor retention and corresponding PTT activity of ICG with nanocarriers that would aggregate in response to an intratumoral enzyme (Figure 3E) [77]. This transition was induced by chemical conversion of peptide pro-gelator NapFFKYp into peptide gelator NapFFKY in the presence of alkaline phosphatase (ALP). The elegant part of the strategy is that ICG molecules were first encapsulated in micelles self-assembled from NapFFKYp, facilitating their transportation in the circulation and penetration into the tumor. Upon contact with ALP in the tumor cells, filaments and then hydrogel started to grow from the enzymatic generated NapFFKY, enabling the continuous deposition and accumulation of ICG in the tumor, reaching as high as 15.05 ± 3.78% ID/g. Taking advantage of this property, the tumor could be clearly visualized by both fluorescence and PA imaging even 24 h after the injection, and complete photothermal ablation of tumor was observed just 2 days after irradiation with an 808 nm laser (0.8 W/cm², 5 min).

As one might note above, ICG was the most used cyanine-based PS for the construction of LTNs, presumably due to its long use as a contrast agent in the clinic and that considerable heat can be generated when it is incorporated into nanoparticles. However, it should be pointed out that free ICG is eliminated from the patients very efficiently while the retention of ICG-based LTNs in the body is much longer. Thus, it is necessary to evaluate the long-term toxicity of ICG when new ICG-based LTNs are tested *in vivo*.

Polymer-based LTNs

Most small molecular PSs, especially porphyrin-based ones, can easily aggregate through π - π stacking due to their hydrophobic and rigid planar structures, a process that favors the dissipation of absorbed energy as heat rather than fluorescence and ¹O₂ generation. Based on this property, Zheng and colleagues created their activatable porphyrin for cancer diagnosis and treatment [41]. An exactly opposite phenomenon exists, termed aggregation induced emission (AIE) [96], which was utilized by Liu and colleagues to produce novel AIE-based LTNs [97-99]. In this case, the PS showed enhanced photoluminescence and production of ROS after they self-assembled into nano-sized aggregates. Unfortunately, current AIE-based LTNs have to be excited with 418 nm light, which is not desirable for *in vivo* application. The absorbance peak of some polymeric PSs could red-shift to the NIR region by taking advantage of the emeraldine base (EB) to the

emeraldine salt (ES) transition during the doping process. Polyaniline, for example, showed strong NIR light absorbance under acidic conditions, and successfully ablated tumor cells and blood vessels in tumor bearing mice when irradiated with an 808 nm laser (2.5 W/cm², 5 min) [39]. The polyaniline, however, requires a PEGylated fatty acid coating and an extra activation process to exert its desired effect. To simplify the system, Yang and colleagues developed a self-doped polymer, PPDS (poly(sodium 3-((3-methyl-3,4-dihydro-2H-thieno[3,4-b][1,4]dioxepin-3-yl)methoxy)propane-1-sulfonate)), which could form stable nanostructures via a surfactant-free one-step process, and provide strong NIR light absorbance under neutral conditions [100]. After surface modification with anti-CD44 antibody, the LTN could be used in the NIR absorbance imaging and PTT of tumors. Nevertheless, the capability for tumor imaging of the NIR-absorbing polymer is not completely satisfactory due to strong background absorbance. To address this issue, enormous effort has been devoted to incorporating additional imaging modules into nanoparticles self-assembled from polypyrrole (PPy), another type of NIR light absorbing polymer [101-103]. For instance, magnetic nanoparticles have been incorporated into PPy-based nanoparticles, allowing simultaneous T_2 -weighted MRI tumor imaging and photothermal tumor ablation [101, 102]. Instead of embedding contrast agents into the core of PPy nanoparticles, Gd could also be introduced into the LTN for T_1 -weighted MRI via covalent modification of PPy with a chelator [103]. The therapeutic effect of PTT could be further augmented when combined with chemotherapy [101].

Other organic LTNs

The potential of other organic PSs in phototherapy have also been explored. These studies focused on the use of PSs that could be easily fabricated into LTNs on a large scale, and on the use of clinically approved dyes for phototherapy. For instance, gallic acid could be easily made into MRI guided LTNs on the gram-scale by reacting with Fe³⁺ in the presence of poly(vinylpyrrolidone) [104]. Prussian blue, a clinical medicine for the treatment of radioactive exposure, has also been used as photothermal agent and contrast agent for PTT and PA imaging of tumor [105]. In addition, new PSs such as boron dipyrromethene (BODIPY)-based photosensitizers are under extensive investigation due to their tunable and sharp excitation/emission spectrum, adjustable singlet-triplet transition, and good photo-chemical properties [12]. The successful development of highly efficient and tunable PSs would greatly advance the area.

Inorganic LTNs

Inorganic nanoparticles possess many unique properties compared with their corresponding bulk materials, among which are their interesting optical properties that are strongly dependent on the particle size [106]. Quantum dots, for example, can emit photons of different energy to that of the excitation radiation, with the emission wavelength determined by the particle size (smaller than the Bohr exciton radius). Additionally, quantum dots exhibit a high quantum yield, superior photostability, long lifetime, and a narrow emission band [107]. In contrast to quantum dots which preferentially emit photons upon irradiation, nanocrystals of noble metals [23] and transition metal chalcogenides [108, 109], and carbon-based materials of zero- [110] one [111] and two-dimensions [112] tend to scatter light or convert light into heat. These unique optical properties allow their utilization as imaging contrast agents and inorganic photothermal agents [113, 114]. Other nanoparticles such as TiO₂ and ZnO have also been reported to generate therapeutic effects under irradiation [28, 29], but UV light is required for excitation and simultaneous tumor imaging is difficult [13, 115]. These inorganic nanoparticles could be used directly or after optimization as LTNs for cancer treatment (Figure 4).

Gold-based LTNs

Noble metals, especially nano-sized gold, have the ability to convert absorbed energy (light) to heat through the LSPR effect [14, 23]. For *in vivo* application, the LSPR frequency of the gold nanoparticle must be tuned to the NIR range for deep tissue penetration, which can be achieved by adjusting the aspect ratio, shell thickness or architecture of the nanoparticles [23, 27]. Early efforts on adjusting the LSPR frequency of gold nanoparticles focused on tuning the shape of gold nanoparticles by making them into nanorods or nanocages [116-119]. Through elongation, the LSPR peak associated with the long axis of the nanorods could be tuned from the visible to NIR range [120]. The formation of nanoshells generates pinholes in the wall, increasing in number as the thickness of the wall decreases, with a concomitant red-shift of the LSPR peak to the NIR range [121, 122]. Their tumor ablation efficacy has been successfully demonstrated on a subcutaneous or orthotopic tumor mouse model when combined with 808 nm laser irradiation [117, 122]. Instead of making hollow cubes, gold nanotubes were recently developed, the LSPR peak of which was tunable via adjustment of the nanotube length [123]. Interestingly, gold quantum dots (~2 nm) also have unique optical and paramagnetic properties compared with gold

nanoparticles. Due to their high surface energy, gold quantum dots have to be stabilized with a mesoporous silica shell, forming a structure called a quantum rattle (QR) (Figure 5A). These QRs could emit NIR fluorescence (812 nm) and generate heat under 672 nm laser irradiation [124], and thus are ideal LTNs capable of tri-modal tumor imaging (fluorescence, MRI and PA imaging) and PTT. Recently, a new gold nanostructure, named the gold beltflower (GBF), was reported by Chen and colleagues, further demonstrating the importance of nanostructure design in photothermal conversion efficiency determination [125]. This GBF contained multiple (>10) branched petals (10 nm in thickness) with long narrow gaps (1–2 nm) between adjacent petals, and a hollow cavity with a wide opening from the conical tip to the scraggly bottom side. Due to the small thickness of the individual petals and the narrow gaps between them, the LSPR of GBFs is greatly enhanced, as evidenced by an ultrahigh photothermal conversion efficiency (74%). Upon intratumoral injection, their presence in the tumor

could be clearly visualized via PA tomography as the generated PA signal could be amplified by their bell-shaped structure. Five minutes tumor irradiation with an 808 nm laser (0.5 W/cm²) was sufficient to achieve complete tumor ablation, while only partial inhibition was observed for gold nanorod treated tumors.

Conventional hollow gold nanoshells and gold nanorods for PTT of tumors are not particularly effective in tumor imaging. Consequently, many additional imaging modalities have been integrated into gold nanoparticles to create multifunctional LTNs. One strategy to construct such an LTN is using nano-sized contrast agents as a core on which to grow a gold shell. For instance, single-walled carbon nanotubes (SWCNT, a SERS probe) [126] and IONP [127–130] have been used to create LTNs that could be used for SERS- or MRI-guided PTT. In contrast to this strategy that introduces additional imaging modalities into the core of gold nanoparticles, another strategy introduces the additional imaging modalities onto the surface instead. In one example, a Raman probe (4-methylbenzenethiol) was conjugated onto the surface of a gold shell, realizing SERS-guided tumor margin determination and localized PTT [131]. In another example, PET imaging modality was incorporated onto the surface of various gold nanoparticles using a chelator-free strategy, allowing the use of gold nanoparticles for PET imaging and PTT of tumors [132]. In this case, ⁶⁴Cu (a PET contrast agent) was chemically reduced on the surface of PEG-stabilized gold nanoparticles of various size and shape. The accumulation of ⁶⁴Cu-labeled gold nanorods in the tumor could be clearly visualized using PET imaging even 45 h after intravenous injection of the ⁶⁴Cu-labeled gold nanorods. Irradiating the tumor with an 808 nm laser (1 W/cm², 10 min) ablated the tumor with negligible recurrence.

The most recent advance in gold nanoparticle-based PTT mainly focused on the use of plasmonic vesicles [27] and other clusters [133]. A plasmonic vesicle is a hollow nanostructure with a membrane assembled from amphiphilic polymer brush-coated metal nanoparticles. These membrane-embedded nanoparticles exhibit strong interparticle plasmonic coupling, resulting in an enhanced electromagnetic field in the interstitial spaces, which significantly amplifies the SERS signal [134] and photo-thermal conversion efficiency for tumor ablation [135–138]. Plasmonic vesicles could be prepared by grafting either amphiphilic block polymers or two types of

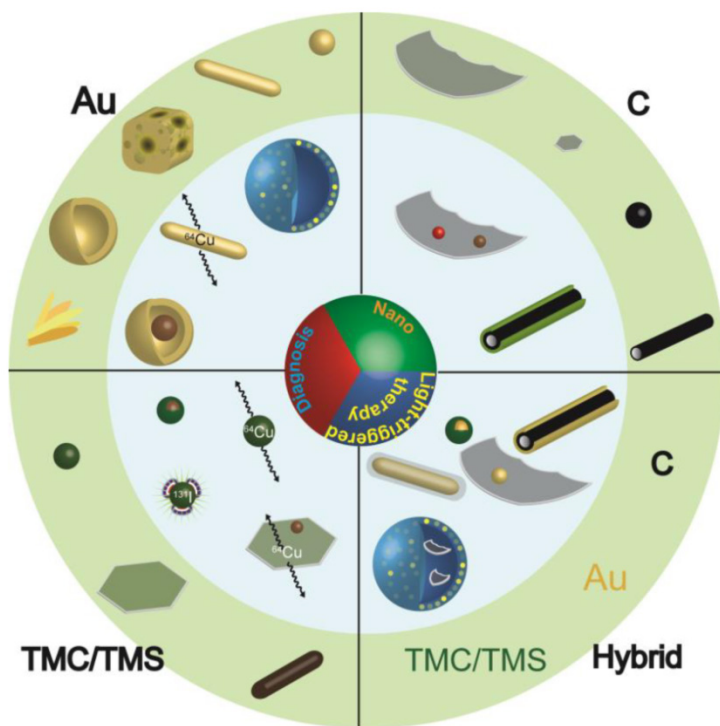


Figure 4. Inorganic LTNs. Schematic illustration of the most explored inorganic LTNs built from gold (Au), transition metal chalcogenides or selenides (TMC/TMS), carbon (C), or hybrids thereof. The structures presented in the light green circle are LTNs built from single materials, and are basic building blocks for more complicated LTNs (light blue circle). LTNs built from gold include nanosphere, nanorod, nanocage, nanoshell, and gold beltflower morphologies (from right to the left), which could be made into plasmonic vesicles, labeled with ⁶⁴Cu or IONPs for enhanced therapeutic and imaging capabilities. LTNs built from TMC/TMS could adopt sphere, sheet, or rod morphologies (from left to right), and could form core/shell structures with IONPs, be labeled with ⁶⁴Cu or ¹³¹I, or doped with IONPs. LTNs made from carbon include graphene, graphene quantum dots, carbon dots, and carbon nanotubes, which could be doped with quantum dots or IONPs, or coated with mesoporous silica for improved tumor imaging or delivery. In addition, hybrid LTNs were created to improve the imaging or therapeutic outcomes, which include Cu₂Ss coated gold spheres, gold-coated carbon nanotubes, graphene-coated gold nanorods, gold nanoparticle-doped graphene, and graphene-loaded plasmonic vesicles.

polymers (one hydrophilic and one hydrophobic) onto one nanoparticle, and then inducing the modified nanoparticles to assemble under optimal conditions [139, 140]. If purposely designed, the assembly and disassembly of plasmonic vesicles could be precisely controlled to realize controllable and traceable drug delivery [134]. The peak of LSPR absorbance could also be precisely tuned by controlling the size of vesicles [136] or the aspect ratio of gold nanoparticles [137]. The peak of LSPR absorbance shifted more toward the NIR region when gold nanorods were used and large vesicles were formed. Along with the red-shift in the LSPR peak, the photothermal conversion efficiency (η) would also increase, enabling their use as PA contrast agent and photothermal agent for tumor imaging and therapy. A recent example of these new gold-based PSs was the plasmonic vesicles self-assembled from PEG and poly(lactic-co-glycolic acid) (PLGA) coated ultrasmall gold nanorods (2 nm in width and 8 nm in length) (Figure 5B) [137]. Vesicles of 60, 80 and 96 nm in diameter were prepared, the LSPR peaks of which shifted to longer wavelength as the vesicle size increased. Upon irradiation with an 808 nm laser (0.8

W/cm²), the tumor treated with gold nanorod vesicles (60 nm) could be clearly visualized using PA tomography, and then ablated completely via PTT. More importantly, the plasmonic vesicle could decompose back into its constituent nanorods that could be efficiently cleared from the body due to their ultrasmall size, avoiding any associated potential long-term toxicity. Chemotherapeutic agents such as doxorubicin could also be encapsulated into the hollow cavity for combination therapy [133].

Gold nanoparticles have attracted much attention due to their unique properties and tunable physiochemical properties (size, shape, surface chemistry). By making them of different size and shape, the peak of LSPR absorbance could be optimized for *in vivo* PTT application, and additional functional modality could be integrated into nanoparticles through rational design. The success in preparing plasmonic vesicles from small nanoparticles allows the fast clearance of gold nanoparticles from the body while retaining their capability as efficient photothermal agents. These findings pave the road to clinical translation of gold nanoparticle-based agents for cancer imaging and therapy. The development of functional polymers that could stabilize these gold-based LTNs and respond to specific stimuli may be one direction that is worthy of exploration.

Transition metal chalcogenide- or selenide-based LTNs

Transition metal chalcogenide (TMC)-based nanostructures are a class of semiconductor nanocrystals with a strong NIR absorbance resulting from nonconventional LSPR [24, 25]. The peaks of LSPR absorbance of the developed TMC nanocrystals lie in the NIR region, and the absorbed energy is mainly dissipated as heat. Thus, TMC nanocrystals are ideal nanomaterials for PTT.

Copper sulfide (CuS) nanoparticles were developed two decades ago [141], and are the most studied TMC nanocrystals so far. The LSPR peak of CuS nanoparticles locates in the 900–1100 nm range of the NIR region, which is desirable for *in vivo* application. However, it was only a few years ago that its photothermal effect and toxicity was actually tested on cells [142]. Compared to gold nanoparticles with NIR absorbance, the size of CuS nanoparticle is much smaller, facilitating its deep tissue penetration and clearance [142–144]. PET contrast agent ⁶⁴Cu could be easily incorporated during the synthesis of nanoparticles without the need for a chelator,

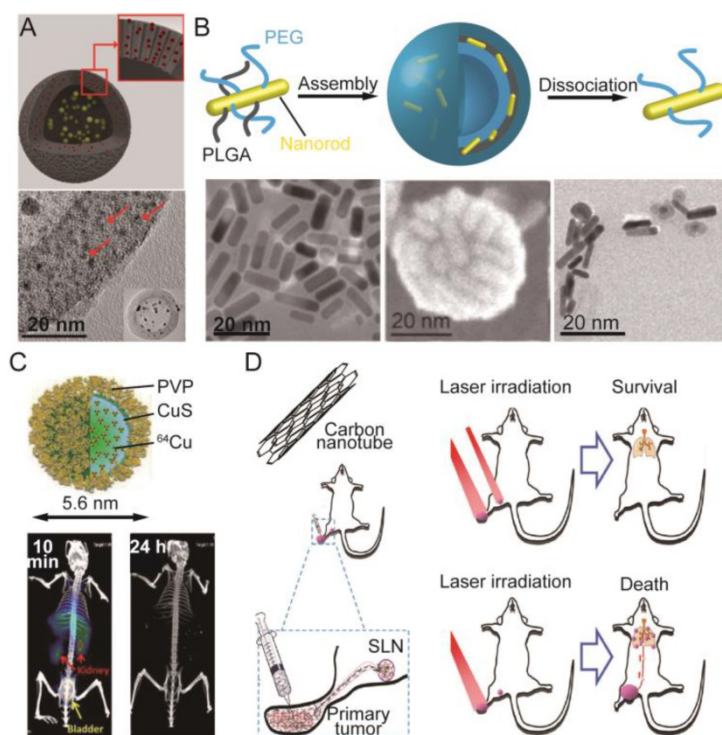


Figure 5. Representative inorganic photosensitizer-based LTNs. (A) Schematic illustration and TEM image of gold-silica quantum rattles. The 2 nm sized gold quantum dots were stabilized in mesoporous silica-based nanoshells. Adapted with permission from [124]. (B) Preparation of plasmonic vesicles from ultrasmall gold nanorods that could dissociate to give PEG-coated gold nanorods after the degradation of PLGA. Adapted with permission from [137]. (C) PVP stabilized ⁶⁴Cu-labeled CuS nanodots with ultrahigh efficient renal clearance as evidenced by time-resolved PET. Adapted with permission from [144]. (D) The use of SWCNTs in the treatment of 4T1 lung metastases. The intratumorally-injected SWCNTs could accumulate in SLNs which together with the primary tumor must be irradiated with a laser to prevent the lung metastasis of the 4T1 tumor and prolong the survival of the animals. Adapted with permission from [173].

allowing PET/CT imaging of its accumulation in the tumor and imaging-guided PTT [145]. Although significant intratumoral accumulation was achieved, large CuS nanoparticles (11 nm in diameter) preferentially accumulated in the liver and spleen, which may cause long-term toxicity to these organs. To address this issue, smaller CuS nanoparticles (5.6 nm in diameter) that could be excreted via the kidneys were synthesized using polyvinylpyrrolidone (PVP) as a stabilizer (Figure 5C) [144]. Their intratumoral accumulation and subsequent clearance could be visualized using PET, and imaging-guided laser irradiation (808 nm, 2 W/cm², 2 min) completely eliminated the tumor without causing any detectable changes in blood biochemistry and hematology. Other imaging modalities could be introduced into CuS nanoparticles by incorporating Mn²⁺ [146], Gd³⁺-UCNP [147], or ¹³¹I [148] into CuS-based LTNs. It is noteworthy that Gd³⁺-UCNP and ¹³¹I, while serving as contrast agents for tumor diagnosis, could also act as sensitizers for or executors of radiotherapy, resulting in a synergistic therapeutic effect [147, 148]. The accumulation of ¹³¹I-doped CuS nanoparticles in sentinel lymph nodes (SLNs) near the primary tumor after intratumoral injection could be visualized using nuclear imaging and CT, which guided the subsequent PTT and radiotherapy on the SLNs after surgical removal of the primary tumor. The combined therapy significantly inhibited the metastasis of tumor to the lungs and prolonged the survival of the model animals [148].

While pursuing CuS nanoparticles with multiple imaging and therapeutic modalities, it is also necessary to improve their tumor targeting capability. Passive, active and externally triggered targeted delivery have all been investigated. Hyaluronic acid-5 β -cholic acid conjugates have been used for CuS encapsulation due to their hydrophilicity and high affinity for CD44 binding [149]. The hyaluronic acid coating facilitated the accumulation of CuS nanoparticle in the tumor through both the EPR effect and hyaluronic acid-CD44 affinity-based active targeting, resulting in improved PA contrast and enhanced PTT efficacy without causing systemic toxicity to the major organs. In order to improve the specificity, the anti-CD105 antibody has been used to increase the intratumoral accumulation of CuS/mesoporous silica core-shell nanoparticles [150]. To track the biodistribution of LTN in real-time with quantitative PET, ⁶⁴Cu-NOTA (1,4,7-triazacyclononanetriacetic acid) was introduced onto their surface. High intratumoral accumulation of this LTN (6%ID/g) was achieved 24 h after intravenous injection. Localized irradiation with a 980 nm laser (4 W/cm², 15 min) completely ablated the tumor

without noticeable toxicity. In addition to the passive and active tumor targeting strategies, an external magnetic field has also been used to increase the tumor deposition of a CuS-based LTN [151]. To achieve this, Fe₃O₄/CuS core-shell LTN (Fe₃O₄@CuS-PEG) was rationally constructed. The Fe₃O₄ core served a dual purpose, navigating the Fe₃O₄@CuS-PEG to the tumor and enabling the T₂-weighted MRI-guided photothermal ablation of tumor.

TMCs can also form single-atom thick sheets that were recently found to be able to convert light into heat [152-160]. The potential of layered TMCs in tumor PTT was first demonstrated using molybdenum sulfide (MoS₂) nanosheets, which were prepared from bulk MoS₂ via weakening of the interlayer forces [152]. Taking advantage of their large surface area for molecular binding, IONPs, ⁶⁴Cu, or chitosan could be deposited onto the surface of MoS₂ nanosheets for multi-modality imaging and drug delivery [153, 154]. Tri-modal imaging (PET, MRI and PA imaging) guided localized laser irradiation (808 nm, 0.78 W/cm², 5 min) was found to completely ablate a xenografted tumor [153], and a synergistic therapeutic effect was achieved when combining PTT with chemotherapy [154]. Aside from the top-down approach, MoS₂ nanosheets could also be synthesized via a bottom-up method (solvothermal treatment) starting from small molecular precursors [155, 156], a process during which an additional functional modality (Bi, an X-ray attenuator) could be incorporated [155]. In addition to MoS₂, tungsten sulfide (WS₂) nanosheets were another layered TMC that proved to be a potent photothermal agent, and could be prepared and modified with similar methods used for MoS₂ [157-159]. Different from MoS₂ and WS₂, both of which must be modified with IONPs to provide contrast for MRI, iron sulfide (FeS) nanoplates themselves can act as both MRI contrast and photothermal agents [161]. PEGylated FeS nanoplates displayed strong superparamagnetism with an *r*₂ relaxivity of 209.8 mM⁻¹s⁻¹ that is much higher than that of IONPs. After intravenous injection of PEGylated FeS nanoplates, the tumor could be clearly identified through T₂-weighted MRI, and then specifically ablated using local laser irradiation (808 nm, 1 W/cm², 5 min).

In addition to spherical and layered structures, TMCs such as bismuth sulfide (Bi₂S₃) could also adopt nanorod shapes. Since Bi is a high Z number element, the high electron density of Bi₂S₃ offers contrast for CT imaging of tumors. Meanwhile, Bi₂S₃ absorbed NIR light strongly with a high photothermal conversion efficiency, and thus was an effective contrast agent for PA imaging and a photothermal agent for tumor

ablation [162].

Transition metal selenides (TMSs) are very similar to sulfide-based TMCs in their photothermal properties. For instance, Bi_2Se_3 is as efficient as Bi_2S_3 in converting light into heat. In work reported by Liu and colleagues, a Bi_2Se_3 -based core/shell LTN ($\text{MnSe}@\text{Bi}_2\text{Se}_3$) was constructed through partial substitution of the surface Mn ions of the MnSe nanocrystals with bismuth [163]. The obtained $\text{MnSe}@\text{Bi}_2\text{Se}_3$ provided contrast for MRI (from MnSe) and CT (from Bi_2Se_3), and enabled precise tumor treatment with radiotherapy (enhanced by Bi_2Se_3) and PTT (from Bi_2Se_3). In this case, the MnSe core mainly served as a contrast agent for MRI. To develop TMSs with an intrinsic capability for MRI, polyacrylic acid-functionalized Co_9Se_8 (PAA- Co_9Se_8 nanoplates) was synthesized as a contrast agent for MRI and PA imaging *in vivo* and as photothermal agent for tumor ablation [164].

LTNs, similar to other nanoparticles for biomedical application, must be precisely tailored with regard to their shape and surface chemistry. TMCs and TMSs are ideal LTNs for cancer diagnosis and therapy, as they can be easily made into nanostructures of differing size, shape and surface chemistry with additional integrated functions. Although the efficacy of these LTNs has been validated *in vivo*, more studies are still required including, but not limited to, the long term toxicity of TMCs and TMSs.

Carbon-based LTNs

Many nanostructures can be formed by carbon, with examples including fullerenes, carbon nanotubes, graphenes, and carbon dots. They have been widely used in many areas such as super strong material fabrication, biomolecule sensing, light harvesting, and drug delivery, due to their superior physicochemical properties and biocompatibility. Since many of these materials can convert light to heat efficiently, they could be used as photothermal agents for cancer therapy as well. Among these materials, carbon nanotubes and graphenes are the two most investigated materials, although the use of other carbon-based LTNs such as carbon dots has also been explored.

Carbon nanotubes are allotropes of carbon with a cylindrical nanostructure, and can be further classified into single-walled carbon nanotubes (SWCNTs) and multiple-walled carbon nanotubes (MWCNTs). SWCNTs are of particular interest for biomedical application as their pharmacokinetic properties have been carefully investigated [165-168]. A pioneering study showed that intratumoral injection of SWCNTs followed with local 808 nm laser

irradiation (76 W/cm^2 , 3 min) could completely ablate the tumor [169]. Despite their successful application in PTT of cancer *in vivo*, the major portion of these as-synthesized SWCNTs were off-resonance under a NIR laser, resulting a low efficiency in photothermal conversion. To address this issue, photo-active (6,5) SWCNTs were purified from the as-synthesized carbon nanotubes using a combination of non-linear density gradient ultracentrifugation (DGU) and a second iterative DGU, followed by stabilization with poly(maleic anhydride-*alt*-1-octadecene)-methoxy poly(ethyleneglycol) ($\text{C}_{18}\text{PMH-PEG}$) [170]. These separated (6,5) SWCNTs exhibited five-fold brighter fluorescence and >10-fold greater efficiency in photothermal conversion, allowing clear tumor visualization (808 nm , 0.14 W/cm^2) and tumor photothermal ablation (980 nm , 0.6 W/cm^2 , 3 min) even at 0.254 mg/kg (*i.v.*). The SWCNTs could be further coated with mesoporous silica and then $\text{C}_{18}\text{PMH-PEG}$ for doxorubicin delivery, achieving combination treatment of cancer with PTT and chemotherapy [171]. The designed LTN also provided contrast for PA tomography and MRI (metal nanoparticles doped on the surface of nanotube during the synthesis served as contrast agent), both of which suggested a good tumor accumulation of the LTN. Local laser irradiation triggered PTT and release of doxorubicin to exert a synergistic effect. While shells coated onto the carbon nanotubes enable the encapsulation of MRI contrast agents and chemotherapeutics, it should be noted that the interface between carbon nanotubes and the shells would affect the magnetic properties of the resulting LTN [172]. In the above cases, the SWCNT was used to eradicate primary tumors. SWCNT-based LTNs could also prevent the metastasis of cancer cells to the lungs (Figure 5D) [173]. Upon intratumoral injection of SWCNT, their accumulation in the tumor and SLNs could be visualized with NIR fluorescence imaging and MRI. Local laser irradiation to the primary tumor completely eradicated the primary tumor, but only with simultaneous irradiation of the SLNs could metastasis of the tumor to the lung be inhibited to realize prolonged survival.

In addition to one-dimensional carbon nanotubes, two-dimensional (2-D) graphene has also attracted tremendous attention in the past few years because of their interesting optical properties (NIR adsorption and fluorescence emission) [53, 174, 175], preferential tumor accumulation in different types of tumors, and low retention in the reticuloendothelial system even 24 h post-injection when compared with PEGylated carbon nanotubes [176]. A single intravenous injection (20 mg/kg) plus localized 808 nm laser irradiation (2 W/cm^2 , 5 min) was sufficient

to achieve complete tumor ablation 2 days after the treatment without recurrence over the course of 40 days. Despite a high intratumoral accumulation, the photothermal efficiency of the non-reduced, covalently PEGylated nanographene oxide was relatively low. Thus, nano-sized, reduced graphene oxide (nano-rGO) was developed, exhibiting a 6-fold increase in NIR absorption compared with nanographene oxide [177], though the nano-rGO only weakly fluoresces as the absorbed energy is preferentially dissipated as heat. To rescue their capability for cancer diagnosis, inorganic functional nanoparticles could be doped onto the surface of graphene to create multifunctional LTNs. For instance, quantum dots [178] and IONPs [179] could be introduced onto the surface of nano-rGO, enabling the use of functionalized nano-rGO as contrast agents for fluorescence imaging, MRI and PA imaging, in addition to their role as a photothermal agent. Gold nanoparticles could be further introduced into the system to provide contrast for X-ray imaging and to improve the photothermal conversion efficiency of nano-rGO for PTT of cancer [180].

Carbon dots [181] and graphene quantum dots (graphene QDs) [182] have recently been used as LTNs for cancer, both of which emit red fluorescence and can kill cancer cells via PTT and PDT, respectively. Carbon dots are quasi-spherical 3D particles with diameters under 10 nm. They were synthesized from polythiophene phenylpropionic acid (PPA) and showed strong photothermal conversion when irradiated with a 671 nm laser (2 W/cm²) [181]. Taking advantage of this property, the carbon dots could be used as a contrast agent for PA imaging and a photothermal agent for PTT of tumors. In contrast to carbon dots, graphene QDs are 2D particles of similar size synthesized from polythiophene derivatives (PT2) [182]. Graphene QDs emitted red fluorescence (695–775 nm) when excited with light of 502–540 nm, and could be used for cancer diagnosis. More importantly, graphene QDs produce ¹O₂ via a multistate sensitization process, resulting in a quantum yield of about 1.3, which makes them a promising photodynamic agent for PDT of cancer.

Carbon-based nanomaterials are a class of materials with great potential in biomedical applications, especially in cancer diagnosis and treatment. They can be structures of zero-, one-, and two-dimensions, with good biocompatibility, high photothermal conversion efficiency or high ¹O₂ yield. More importantly, additional functional modalities can be integrated into these carbon-based nanostructures to obtain multifunctional LTNs.

Despite the success, their heterogeneity is still a big challenge for these materials before their clinical translation. For instance, SWCNTs are a mixture of nanotubes with different lengths and diameters, the majority of which will be off-resonance under laser irradiation, and the prepared graphenes typically have metal nanoparticles deposited on the surface. It is thus necessary to obtain carbon nanomaterials with well-defined physicochemical properties.

Hybrid LTNs

In addition to LTNs composed of one type of PS, many hybrid LTNs have been developed. One reason to build hybrid LTNs is that the efficacy of photothermal conversion could be greatly improved when putting two PSs into a single nanoparticle. For example, after being coated with rGO on the surface, the electromagnetic field around gold nanorods exhibits a four-fold enhancement that improves the photothermal conversion [183]. Other than rGO, Cu₉S₅ could also be coated onto the surface of a gold nanoparticle (Figure 6A) [184]. The constructed Au@Cu₉S₅ nanoparticles had a well-controlled interface between the core and shell, and a strong coupling of the collective hole oscillation in the heavily doped Cu₉S₅ with the surface-enhanced near-field of the noble gold nanoparticles was observed, evidenced by superior photothermal conversion efficiency (37%) under irradiation with a 1064 nm laser (second NIR window). In addition to building hybrid LTNs with core/shell structures, the encapsulation of rGO into plasmonic vesicles could also improve the photothermal conversion efficiency (Figure 6B). In this case, doxorubicin and doxorubicin-loaded rGO was loaded into the hollow cavity of plasmonic vesicles [138]. The incorporation of rGO into the plasmonic vesicles improved the photothermal performance of the hybrid LTN as rGO itself is a photothermal agent whose photothermal conversion capability could be greatly improved if it is adjacent to plasmonic nanoparticles [183, 185]. At the same time, doxorubicin adsorbed on the surface of rGO would release in an acidic environment upon irradiation with the laser (e.g. in lysosomes). Due to the greatly enhanced photothermal conversion efficiency of the system and sequential release of encapsulated doxorubicin (first non-rGO adsorbed and then rGO adsorbed), the tumor could be clearly visualized with PA tomography, and be ablated with a single intravenous injection of the LTN followed by low-power-density 808 nm laser irradiation (0.25 W/cm²).

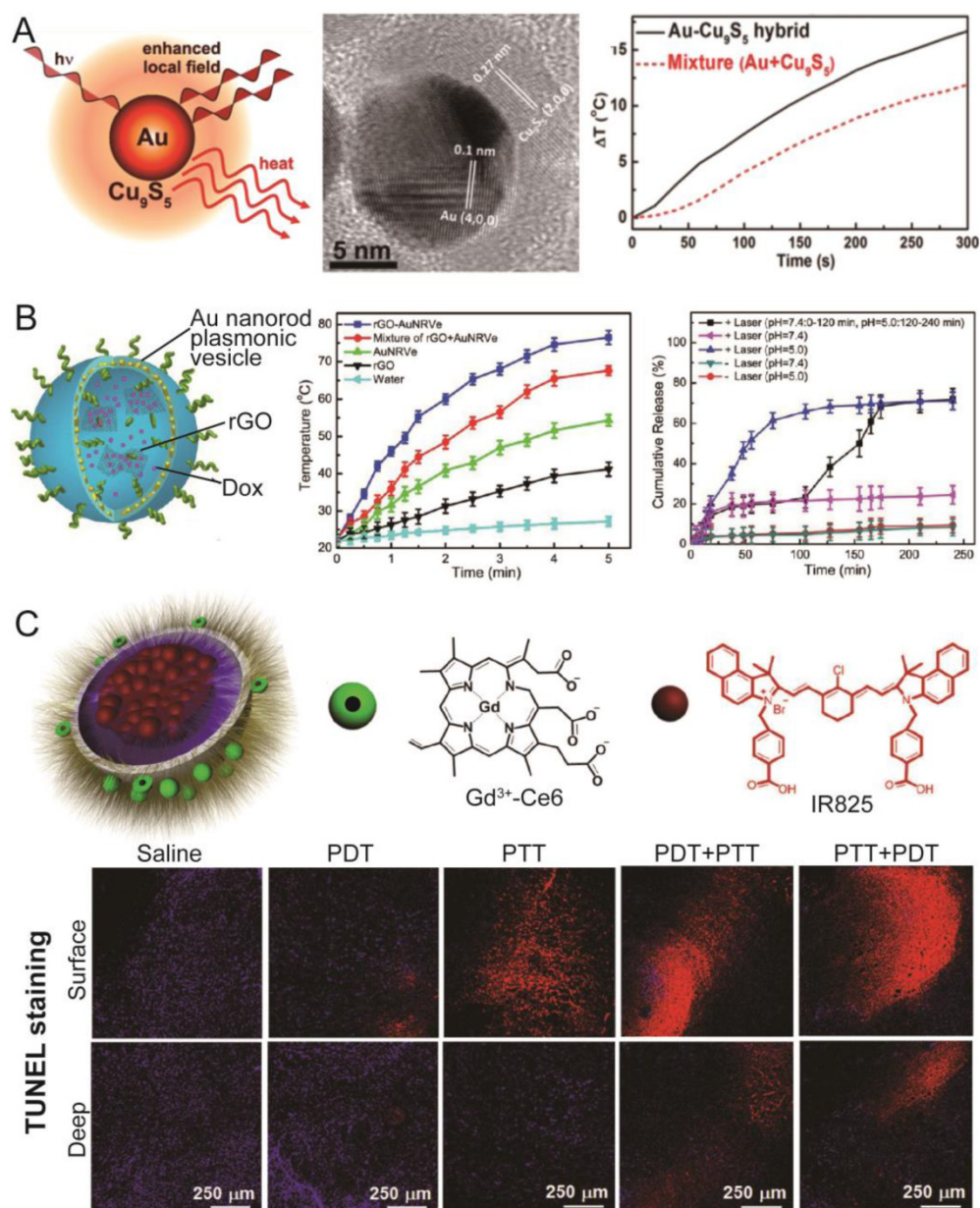


Figure 6. Representative hybrid LTNs. (A) The schematic illustration and TEM image of a Au-Cu₃S₅ core-shell LTN. This core-shelled LTN showed an improved photothermal conversion efficiency compared with the mixture of Au nanoparticles and Cu₃S₅ nanoparticles at the same concentrations. Adapted with permission from [184] (B) Schematic illustration of Au nanorod plasmonic vesicles loaded with rGO and Dox (rGO-AuNRVe-DOX). rGO-AuNRVe-DOX showed improved photothermal conversion efficiency, and the release of Dox from the vesicles could be accelerated by lowering the pH, with laser irradiation, or a combination of the two. Adapted with permission from [138]. (C) Schematic illustration of IR825-loaded and Gd³⁺-Ce6-conjugated micelles with two therapeutic modalities (PDT and PTT). Treating the tumor sequentially with PTT and PDT was the most effective method for inducing the apoptosis of cancer cells, as evidenced by TUNEL staining. Adapted with permission from [186].

Another reason to develop hybrid LTNs is that two modalities (PDT and PTT) could be integrated into one nanoparticle. As mentioned previously, PDT, while very effective in cancer cell ablation, requires the presence of oxygen to exert its effect. PTT does not require the presence of oxygen, but a high power laser and prolonged irradiation were needed for PTT to heat the tumor to the threshold temperature. It has been reported that hyperthermia can, in addition to its cell killing capability, improve the blood flow and sensitize the cancer cells to other treatments [18], and thus a synergistic effect between PDT and PTT is

expected. Such LTNs could be constructed from two organic PSs or one organic and one inorganic PS. Liu and colleagues used micelles self-assembled from Gd³⁺-Ce6-conjugated PEG-grafted poly(maleic anhydride-alt-1-octadecene) (C₁₈PMH-PEG-Ce6-Gd) to encapsulate the photothermal agent IR825 (Figure 6C) [186]. The resulting LTN successfully accumulated in subcutaneous xenograft 4T1 tumors in mice, as evidenced by fluorescence imaging and MRI, and the perfusion of the tumor could be monitored through PA tomography by taking advantage of the photothermal effect of IR825. Furthermore, the

sequential application of PTT and PDT significantly inhibited the tumor growth compared with PDT or PTT monotherapy or the sequential application of PDT and PTT. A similar synergistic therapeutic outcome could also be achieved by encapsulating Ce6 and cyanine dye into a single micelle, an LTN that also proved useful for dual-modality tumor imaging (fluorescence imaging and PA tomography) [187]. Ce6 has also been combined with a PPy nanoparticle to construct an LTN with both PDT and PTT modalities. In this case, Gd³⁺-Ce6-conjugated bovine serum albumin was used as a stabilizer of PPy nanoparticles [188]. The elegant design of this LTN realized simultaneous dual-modality T₁-weighted MRI and fluorescence imaging, and specific and potent tumor ablation through PDT and PTT.

Hybrid LTNs composed of both organic and inorganic PS can be easily created by using an inorganic PS as a carrier for an organic PS or by using a second nanoparticle to carry both PSs. For instance, polymer-coated gold nanorods could be used as carriers for ICG [118, 189] or Al(III)-phthalocyanine chloride tetrasulfonic acid (AIPcS4) [190]. Nanographenes (photothermal agents) could deliver ZnPc, a photosensitizer, to realize PDT/PTT-mediated tumor ablation [191]. The recently developed plasmonic vesicles are another ideal carrier for Ce6 to effect PDT/PTT dual-modality treatment [135]. Significant advantages were observed when comparing combination therapy with monotherapy. In addition to these works, Lin and colleagues used a GdOF:Ln@SiO₂ framework as a carrier for doxorubicin, ZnPc and carbon dots to realize tri-modal cancer therapy [192]. The UCNP core (GdOF:Ln) converted NIR laser into red light which excited the ZnPc and carbon dots to generate ¹O₂ and heat. The latter, while eradicating the tumor via hyperthermia, could also accelerate the release of doxorubicin for chemotherapy.

It is apparent that creating hybrid LTNs is a feasible and effective way to realize multiple functions that are otherwise difficult to achieve with a single PS. Taking advantage of developments in nanotechnology, the fabrication of nano-sized objects with well-controlled physical properties is becoming easier. However, one should always balance the benefits and costs when designing and synthesizing these smart LTNs.

Discussion

Over the past several years, a great many advances have been made in the design and application of LTN in cancer diagnosis and therapy, and many novel and promising LTNs have been created (Table 1). Among the PSs that have been used

to construct LTNs, organic PSs (such as porphyrin- and cyanine-based PSs) are the most used, presumably due to their good biocompatibility, low toxicity and their utility in both PTT and PDT. In addition, the fluorescence emitted by small molecular PSs could be used in tumor imaging. In most cases, porphyrin-based PSs were used as photodynamic agents and contrast agents for MRI or PET, showing potent efficacy against both subcutaneous and orthotopic tumors. Nevertheless, porphyrin-based PSs have to be excited with ~700 nm laser radiation unless they are used in combination with UCNPs, limiting their application in the treatment of deeply located tumors. Different from porphyrin-based PSs, other organic PSs are photothermal agents that can be effectively excited with 808 nm laser radiation, allowing for deeper tissue penetration [193]. They are mainly used as contrast agents for PA tomography and therapeutic agents for PTT. Similarly, inorganic PS-based LTNs kill cancer cells through PTT, but have their own advantages when compared with organic PSs. For instance, the LSPR peaks of inorganic PSs mainly locate at 808 nm or longer, which is desirable for *in vivo* application. Furthermore, additional imaging (MRI, CT and PET) and therapeutic modalities (chemotherapy or radiotherapy) can be easily introduced into or onto inorganic PSs via a covalent or non-covalent strategy. Despite these advantages, the safety of inorganic LTNs is the major concern for their clinical application. To address this issue, inorganic LTNs with fast clearance were developed, as well as hybrid LTNs combining two or more PSs working synergistically, through which the exposure and the potential toxicity of these inorganic LTN could be reduced while retaining their anti-tumor activity.

Light-triggered therapy, while effective for eradicating cancer cells, also induces post-treatment effects that could improve the efficacy of combined treatments through enhanced intratumoral penetration and cellular entry of nanoparticles, accelerated drug release, and a boosted immune response against cancer cells [194-197]. For instance, ¹O₂ generated by an RGD-modified ferritin-based LTN could kill the endothelial cells in the tumor, further permeabilizing the leaky tumor vessels [195]. This EPR enhancement technology increased the intratumoral accumulation of a subsequently injected nanomedicine by as much as 20-fold. It has been reported that the heating of tumors up to 42 °C could make the cancer cells more susceptible to other treatments [18]. One possible reason for this is that the permeability of the cell membrane and endocytosis of nanoparticles is higher at 42 °C than at 37 °C [196]. Local hyperthermia in the tumor would also damage

the vasculature in the tumor, which would affect the distribution of subsequently dosed drugs [198]. More importantly, tumor-associated antigens released by LTN-destroyed tumor cells, could be processed and presented by dendritic cells stimulated by LNT, resulting in a profound immunological response

against the tumor especially when combined with anti-CTLA-4 antibody which could abrogate regulated T cells at distant tumor [197]. It is clear that synergistic therapeutic effects can be achieved when combining LNTs with other therapeutic modalities such as chemotherapy and immunotherapy.

Table 1. Brief summary of the recently developed LTNs.

LTN	Photosensitizer	Laser (nm)	Tumor model	Imaging modality	Therapeutic modality	Refs.
Porphyrin-based LTN	Pyropheophorbide	680	Orthotopic head and neck tumor, subcutaneous KB tumor	FI, PA	PTT	[41, 42]
	BPD	690	Orthotopic and subcutaneous AsPC1 tumor	FI	PDT, Ch	[44]
	Purpurin18	730	Subcutaneous U87-MG tumor	PA	PTT	[45]
	Porphyrin	671	Orthotopic U87-MG and PC-3 tumor	FI, PET/CT	PDT	[51]
	Ce6	430, 660, 670, 671, 704, 808 ^a , 980 ^a	Subcutaneous HeLa, MDA-MB-435, HT-29, 4T1, HCT-116, CT26, U87-MG, or MGC803 tumor	FI, PA, MRI	PDT	[46-48, 56, 58, 60, 63, 65, 67, 68, 71]
	Protoporphyrin IX	633	Subcutaneous HT-29 tumor	FI	PDT	[47]
	5,10,15,20-tetra (4-pyridyl) porphyrin	635	Subcutaneous A549 tumor	FI	PDT, Ch	[50]
	Sinoporphyrin sodium	630	Subcutaneous U87-MG tumor	FI	PDT	[54]
	ZnPc	660, 980 ^a	Subcutaneous HeLa, or Bel-7402 tumor	FI	PDT	[55, 66]
Cyanine-based LTN	Hematoporphyrin	980 ^a	Subcutaneous 4T1 tumor	FI, MRI	PDT, Ch, Ra	[69]
	IR780	808	Subcutaneous MCF-7 or HCT-116 tumor	FI, PET/CT	PTT	[76, 88]
	ICG	785, 808	Subcutaneous HeLa, 4T1, A549, MCF-7 or MCF-7/ADR tumor	FI, PA, MRI	PDT, PTT, Ch	[77, 78, 80, 82, 85, 86, 89, 91]
	IR820	808	Subcutaneous 4T1 tumor	FI, PA	PTT	[81]
	Cy5COOH	808	Subcutaneous 4T1 tumor	FI, PA	PTT	[83]
	Cypate	785	Subcutaneous 4T1 tumor	FI, PA, MRI	PTT	[84]
	DiR	808	Subcutaneous 4T1 tumor	FI, PA	PTT	[87]
Other organic LTN	IR825, Rose Bengal	808, 980 ^a	Subcutaneous 4T1 tumor	FI, MRI	PDT, PTT	[90]
	Polyaniline	808	Subcutaneous A431 tumor	NIR absorbance	PTT	[39]
	PPDS	808	Subcutaneous MDA-MB-231 tumor	NIR absorbance	PTT	[100]
	PPy	808	Subcutaneous 4T1 or U87-MG tumor	PA, MRI	PTT, Ch	[101-103]
	Gallic acid	808	Subcutaneous SW620 tumor	MRI	PTT	[104]
Au-based LTN	Prussian blue	808	Subcutaneous HeLa tumor	PA, Ultrasound	PTT, Ch	[105]
	Au nanocages	808	Subcutaneous U87-MGwt EGFR tumor	-	PTT	[117]
	Au nanocapsule	808	Orthotopic U87-MG tumor	FI, PET/CT	PTT	[122]
	Au nanotubes	800	Subcutaneous SW620 and HCT116 tumor	PA	PTT	[123]
	Au quantum dots	672	Subcutaneous LS174T-luc tumor	FI, PA, MRI	PTT	[124]
	Au beltflower	808	Subcutaneous 4T1 tumor	PA	PTT, Ch	[125]
	Au nanoshells	808	Subcutaneous HeLa and MCF-7 tumor	MRI	PTT	[127]
	γFe ₂ O ₃ @Au	808	Subcutaneous 4T1 tumor	PA, MRI, SERS	PTT	[131]
	Au-NP	808	Subcutaneous U87-MG tumor	PET	PTT	[132]
TMC or TMS-based LTN	Au-NP NV	808	Subcutaneous MDA-MB-435 tumor	PA	PTT	[136]
	Au-NR NV	808	Subcutaneous U87-MG tumor	PA, PET	PTT	[137]
	CuS nanoparticles	808, 980 ^a , 1064	Orthotopic U87-MG or 4T1 tumor Subcutaneous U87-MG, MDA-MB-231, 4T1, or SCC7 tumor	FI, PA, MRI, PET, CT, γ-imaging	PTT, Ra	[143, 145-149]
	CuS nanodots	808	Subcutaneous and orthotopic 4T1 tumor	PET/CT	PTT	[144]
	CuS@MSN	808, 980, 1064	Subcutaneous 4T1 or HeLa tumor	PA, MRI	PTT	[150, 151]
	MoS ₂ nanosheets	808	Subcutaneous 4T1 or Panc-1 tumor	PA, MRI, PET, CT	PTT, Ch, Ra	[153-156]
	WS ₂	808	Subcutaneous Panc-1 or 4T1 tumor	FI, PA, MRI, CT	PTT, Ch	[157-159]
	FeS	808	Subcutaneous 4T1 tumor	MRI	PTT	[161]
	Bi ₂ S ₃	808	Subcutaneous 4T1 tumor	PA, CT	PTT	[162]
	MnSe@Bi ₂ Se ₃	808	Subcutaneous 4T1 tumor	MRI, CT	PTT, Ra	[163]
	Co ₉ Se ₈	808	Subcutaneous HepG2 tumor	PA, MRI	PTT	[164]
Carbon-based LTN	SWCNT	808	Subcutaneous or metastasized 4T1 tumor	FI, PA, MRI, SERS	PTT, Ch	[170, 171, 173]
	Nanographene	808	Subcutaneous 4T1 tumor	FI	PTT	[176]
	rGO-IONP	808	Subcutaneous 4T1 tumor	FI, PA, MRI	PTT	[179]
	GO-IONP-Au	808	Subcutaneous 4T1 tumor	MRI, CT	PTT	[180]
	Carbon dots	671	Subcutaneous HeLa tumor	FI, PA	PTT	[181]
Hybrid LTN	Graphene QDs	502-540	Subcutaneous MDA-MB-231-GFP tumor	FI	PDT	[182]
	Au@Cu ₂ S	1064	Subcutaneous CT26 tumor	CT	PTT	[184]
	rGO@Au-NR NV	808	Subcutaneous U87-MG tumor	PA, PET	PTT, Ch	[138]
	Gd ³⁺ -Ce6, IR825	808	Subcutaneous 4T1 tumor	FI, PA, MRI	PDT, PTT	[186]
	Cypate, Ce6	660, 785	Subcutaneous 4T1 tumor	FI, PA	PDT, PTT	[187]
	PPy@BSA-Ce6	660, 808	Subcutaneous 4T1 tumor	FI, MRI	PDT, PTT	[188]
ICG, Au-NR	808	Subcutaneous H22 tumor	FI	PDT, PTT	[189]	

	GNR-AIPc54	670, 810	Subcutaneous SCC7 tumor	FI	PDT, PTT	[190]
	Au-NP NV-Ce6	671	Subcutaneous MDA-MB-435 tumor	FI, PA	PDT, PTT	[135]
	GdOF:Ln@SiO ₂	980 ^a	Subcutaneous H22 tumor	FI, MRI, CT	PDT, PTT, Ch	[192]
	ZnPc-carbon dots					

^a Upconversion nanoparticles were used in LTN construction.

FI, fluorescence imaging; PA, photoacoustic tomography; MRI, magnetic resonance imaging; PET, positron emission tomography; CT, computed tomography; SERS, surface enhanced Raman scattering; PDT, photodynamic therapy; PTT, photothermal therapy; Ch, chemotherapy; Ra, radiotherapy.

Conclusion and perspectives

Precision medicine has been recognized as one of the future directions for medicine research and development, as it is becoming more and more evident that the incidence and status of a cancerous disease in one patient can be very different to that in others, as is the response to any treatment. Among the many strategies to realize precision medicine, the development of LTNs presents a feasible means to convert current “one fits all” treatments into personalized approaches [4, 38]. The imaging modality allows the detection of disease sites and predicts whether the patient will benefit from the treatment, while the light-triggered therapeutic modality could be localized in and around the diseased tissue without resulting in any significant off-target toxicity. In addition, the same LTN could be used to monitor the outcome of the therapy, and the second treatment could be initiated or adjusted accordingly. As detailed in the present review, many great advances have been achieved in the development of LTNs for cancer therapy within the past few years, with both their diagnosis and therapeutic capabilities validated on tumor-bearing animal models. In most cases, complete tumor ablation was achieved and synergistic effects were often observed when the LTN was combined with other therapeutic modalities. Currently, several light-triggered therapies are already in clinical use for the treatment of some superficial cancers, achieving good therapeutic effect, though the occurrence of phototoxicity due to the non-specific accumulation of PS in the skin remains a problem [40]. Fortunately, a number of nanomedicines have been approved for clinical use, showing improved specificity and efficacy compared with the respective free drugs. One such example is Visudyne®, a liposomal formulation of verteporfin (porphyrin-based PS) that suffers from poor bioavailability [199]. Taking advantage of advances in nanotechnology, it can be foreseen that the limitations currently hampering the application of PSs will be overcome, and that the clinical translation of LTNs is highly expected.

Despite the promising results and future, several technical challenges must be overcome before the clinical translation of LTNs can be realized. One critical challenge is that current LTNs are of low

efficiency with noteworthy side effects, which are mainly due to the low photothermal conversion and ¹O₂ generation efficiency of PSs, and the poor tumor-specific accumulation of LTNs. Another challenge is the poor tissue penetration of the laser radiation required for LTN activation that hampers the treatment of deeply located tumors. Longer wavelength lasers can penetrate deeper into the tissue, but the choice of the laser is dictated by the photophysical properties of the chosen PS. The tissue penetration efficiency and PS activation efficiency must thus be balanced if the highest anti-tumor activity is to be achieved. Toxicity is another big challenge for the clinical translation of LTNs, especially for inorganic nanoparticle-based LTNs which might persist for months in the body and cause toxicity to cells [200, 201].

To overcome these challenges, LTNs should be improved in several aspects. First, new PSs, laser sources and light delivery methods should be developed. As the key component of an LTN, PSs that absorb longer wavelength radiation and achieve high photothermal conversion and/or ¹O₂ generation efficiency are highly desired to effectively treat deeply located tumors. For instance, CuS nanoparticles with strong absorption at 1064 nm could be visualized with PA tomography even if it was buried beneath tissue up to 5 cm in thickness [143]. For PSs that absorb at shorter wavelengths, it is also possible to treat deeply located tumors through combination use with UCNPs [61] or by using two-photon excitation technology [202]. In addition, it is also necessary to develop new light delivery techniques that could realize PS activation in deep tissues, with one possible strategy being the design of implantable NIR light sources [203]. Second, LTNs with tumor-specific accumulation are required. Most of the reported LTNs realized their tumor accumulation through the EPR effect, and tumor specific treatment was then administered via local tumor irradiation with a laser. However, non-specifically deposited LTNs composed of porphyrin-based PSs or inorganic particles would exert toxicity, as the former would be activated if irradiated with UV or visible light [72], and the latter could cause long-term toxicity to other organs especially when repeated dosing is required. Thus, it is necessary to improve the specificity of LTNs with strategies such as active targeting and to accelerate the

clearance of LTNs (especially inorganic LTNs) by reducing their size [27, 144]. Third, more clinically-relevant tumor models should be used for LTN evaluation. Subcutaneous xenograft tumor models were predominantly used for LTN evaluation (Table 1), but many human tumors are deeply embedded beneath other tissues. The accumulation of LTNs in the orthotopic tumor and the accessibility of laser to the tumor should be systemically tested. Fourth, the potential of LTNs against tumor metastases has not been extensively explored. Tumor metastasis is the major cause of death for cancer patients, but current work on LTNs focused mainly on the treatment of primary tumors. LTNs that can detect, prevent and eradicate tumor metastases are greatly needed. Rational design of LTNs that are able to exert both potent and transitory PDT/PTT and long lasting chemotherapy or immunotherapy might be a future direction. Lastly, the potential of LTNs in cancer diagnosis has not been fully explored. The imaging modality in current LTNs was mainly used to track the biodistribution of LTNs and to guide the subsequent phototherapy. It is effective but not enough to realize precision medicine which requires the expression profiles of cancer biomarkers to be detected in order to guide further treatment. In summary, LTNs have already demonstrated great potential in cancer therapy, and continuous progress in the field is expected. Multifunctional LTNs with balanced costs and benefits will make a great impact to cancer treatment in the near future.

Acknowledgements

We thank The National Natural Science Foundation of China (81521005, 81270047), The National Basic Research Program of China (2012CB932502, 2013CB932503), and Shanghai Pujiang program (15PJ1409900) for financial support. We also thank Dr. Andrew G. Cheetham for the critical reading.

Competing Interests

The authors have declared that no competing interest exists.

References

- Torre LA, Bray F, Siegel RL, et al. Global cancer statistics, 2012. *CA Cancer J Clin.* 2015; 65: 87-108.
- Bedard PL, Hansen AR, Ratain MJ, et al. Tumour heterogeneity in the clinic. *Nature.* 2013; 501: 355-64.
- Hanahan D, Weinberg RA. Hallmarks of cancer: the next generation. *Cell.* 2011; 144: 646-74.
- Mura S, Couvreur P. Nanotheranostics for personalized medicine. *Adv Drug Deliv Rev.* 2012; 64: 1394-416.
- Cheng Z, Al Zaki A, Hui JZ, et al. Multifunctional nanoparticles: cost versus benefit of adding targeting and imaging capabilities. *Science.* 2012; 338: 903-10.
- Koo H, Huh MS, Sun IC, et al. In vivo targeted delivery of nanoparticles for theranosis. *Acc Chem Res.* 2011; 44: 1018-28.
- Chen Q, Ke H, Dai Z, et al. Nanoscale theranostics for physical stimulus-responsive cancer therapies. *Biomaterials.* 2015; 73: 214-30.
- Zhang P, Cheetham AG, Lock LL, et al. Activatable nanoparticles for biomolecular detection. *Curr Opin Biotechnol.* 2015; 34: 171-9.
- Tong HJ, Lou KY, Wang W. Near-infrared fluorescent probes for imaging of amyloid plaques in Alzheimer's disease. *Acta Pharm Sin B.* 2015; 5: 25-33.
- Agostinis P, Berg K, Cengel KA, et al. Photodynamic therapy of cancer: an update. *CA Cancer J Clin.* 2011; 61: 250-81.
- Josefsen LB, Boyle RW. Unique diagnostic and therapeutic roles of porphyrins and phthalocyanines in photodynamic therapy, imaging and theranostics. *Theranostics.* 2012; 2: 916-66.
- Auwah SG, You Y. Boron dipyrromethene (BODIPY)-based photosensitizers for photodynamic therapy. *Rsc Advances.* 2012; 2: 11169-83.
- Lucky SS, Soo KC, Zhang Y. Nanoparticles in photodynamic therapy. *Chem Rev.* 2015; 115: 1990-2042.
- Dykman L, Khlebtsov N. Gold nanoparticles in biomedical applications: recent advances and perspectives. *Chem Soc Rev.* 2012; 41: 2256-82.
- Zhang Z, Wang J, Chen C. Near-infrared light-mediated nanoplatforams for cancer thermo-chemotherapy and optical imaging. *Adv Mater.* 2013; 25: 3869-80.
- Ng KK, Zheng G. Molecular interactions in organic nanoparticles for phototheranostic applications. *Chem Rev.* 2015; 115: 11012-42.
- Welsher K, Liu Z, Darancioglu D, et al. Selective probing and imaging of cells with single walled carbon nanotubes as near-infrared fluorescent molecules. *Nano Lett.* 2008; 8: 586-90.
- Hildebrandt B, Wust P, Ahlers O, et al. The cellular and molecular basis of hyperthermia. *Crit Rev Oncol Hematol.* 2002; 43: 33-56.
- Hatz S, Lambert JD, Ogilby PR. Measuring the lifetime of singlet oxygen in a single cell: addressing the issue of cell viability. *Photochem Photobiol Sci.* 2007; 6: 1106-16.
- Davies MJ. Singlet oxygen-mediated damage to proteins and its consequences. *Biochem Biophys Res Commun.* 2003; 305: 761-70.
- Chen Z, Tabakman SM, Goodwin AP, et al. Protein microarrays with carbon nanotubes as multicolor Raman labels. *Nat Biotechnol.* 2008; 26: 1285-92.
- Farhadi A, Roxin A, Wilson BC, et al. Nano-enabled SERS reporting photosensitizers. *Theranostics.* 2015; 5: 469-76.
- Jain PK, Huang XH, El-Sayed IH, et al. Noble metals on the nanoscale: optical and photothermal properties and some applications in imaging, sensing, biology, and medicine. *Acc Chem Res.* 2008; 41: 1578-86.
- Luther JM, Jain PK, Ewers T, et al. Localized surface plasmon resonances arising from free carriers in doped quantum dots. *Nat Mater.* 2011; 10: 361-6.
- Xie Y, Carbone L, Nobile C, et al. Metallic-like stoichiometric copper sulfide nanocrystals: phase- and shape-selective synthesis, near-infrared surface plasmon resonance properties, and their modeling. *ACS Nano.* 2013; 7: 7352-69.
- Melancon MP, Zhou M, Li C. Cancer theranostics with near-infrared light-activatable multimodal nanoparticles. *Acc Chem Res.* 2011; 44: 947-56.
- Song J, Huang P, Duan H, et al. Plasmonic vesicles of amphiphilic nanocrystals: optically active multifunctional platform for cancer diagnosis and therapy. *Acc Chem Res.* 2015; 48: 2506-15.
- Cai RX, Kubota Y, Shuin T, et al. Induction of cytotoxicity by photoexcited TiO₂ particles. *Cancer Res.* 1992; 52: 2346-48.
- Hackenberg S, Scherzed A, Kessler M, et al. Zinc oxide nanoparticles induce photocatalytic cell death in human head and neck squamous cell carcinoma cell lines in vitro. *Int J Oncol.* 2010; 37: 1583-90.
- Mura S, Nicolas J, Couvreur P. Stimuli-responsive nanocarriers for drug delivery. *Nat Mater.* 2013; 12: 991-1003.
- Priya James H, John R, Alex A, et al. Smart polymers for the controlled delivery of drugs - a concise overview. *Acta Pharm Sin B.* 2014; 4: 120-7.
- Carter KA, Shao S, Hoopes MI, et al. Porphyrin-phospholipid liposomes permeabilized by near-infrared light. *Nat Commun.* 2014; 5: 3546.
- Luo D, Carter KA, Razi A, et al. Doxorubicin encapsulated in stealth liposomes conferred with light-triggered drug release. *Biomaterials.* 2016; 75: 193-202.
- Dai Y, Xiao H, Liu J, et al. In vivo multimodality imaging and cancer therapy by near-infrared light-triggered trans-platinum pro-drug-conjugated upconversion nanoparticles. *J Am Chem Soc.* 2013; 135: 18920-9.
- Dougherty TJ, Grindey GB, Fiel R, et al. Photoradiation therapy .2. cure of animal tumors with hematoporphyrin and light. *J Natl Cancer Inst.* 1975; 55: 115-21.
- Song XJ, Chen Q, Liu Z. Recent advances in the development of organic photothermal nano-agents. *Nano Research.* 2015; 8: 340-54.
- Fuhrmann G, Serio A, Mazo M, et al. Active loading into extracellular vesicles significantly improves the cellular uptake and photodynamic effect of porphyrins. *J Control Release.* 2015; 205: 35-44.
- Rai P, Mallidi S, Zheng X, et al. Development and applications of photo-triggered theranostic agents. *Adv Drug Deliv Rev.* 2010; 62: 1094-124.
- Yang J, Choi J, Bang D, et al. Convertible organic nanoparticles for near-infrared photothermal ablation of cancer cells. *Angew Chem Int Ed Engl.* 2011; 50: 441-4.
- Ethirajan M, Chen Y, Joshi P, et al. The role of porphyrin chemistry in tumor imaging and photodynamic therapy. *Chem Soc Rev.* 2011; 40: 340-62.
- Lovell JF, Jin CS, Huynh E, et al. Porphyrin nanovesicles generated by porphyrin bilayers for use as multimodal biophotonic contrast agents. *Nat Mater.* 2011; 10: 324-32.
- Muhanna N, Jin CS, Huynh E, et al. Phototheranostic porphyrin nanoparticles enable visualization and targeted treatment of head and neck cancer in clinically relevant models. *Theranostics.* 2015; 5: 1428-43.

43. Huynh E, Leung BY, Helfield BL, et al. In situ conversion of porphyrin microbubbles to nanoparticles for multimodality imaging. *Nat Nanotechnol.* 2015; 10: 325-32.
44. Spring BQ, Bryan Sears R, Zheng LZ, et al. A photoactivable multi-inhibitor nanoliposome for tumour control and simultaneous inhibition of treatment escape pathways. *Nat Nanotechnol.* 2016; doi:10.1038/nnano.2015.311.
45. Zhang D, Qi GB, Zhao YX, et al. In situ formation of nanofibers from Purpurin18-peptide conjugates and the assembly induced retention effect in tumor sites. *Adv Mater.* 2015; 27: 6125-30.
46. Park SY, Baik HJ, Oh YT, et al. A smart polysaccharide/drug conjugate for photodynamic therapy. *Angew Chem Int Ed Engl.* 2011; 50: 1644-7.
47. Lee SJ, Koo H, Lee DE, et al. Tumor-homing photosensitizer-conjugated glycol chitosan nanoparticles for synchronous photodynamic imaging and therapy based on cellular on/off system. *Biomaterials.* 2011; 32: 4021-9.
48. Yoon HY, Koo H, Choi KY, et al. Tumor-targeting hyaluronic acid nanoparticles for photodynamic imaging and therapy. *Biomaterials.* 2012; 33: 3980-9.
49. Cheng Y, Meyers JD, Broome AM, et al. Deep penetration of a PDT drug into tumors by noncovalent drug-gold nanoparticle conjugates. *J Am Chem Soc.* 2011; 133: 2583-91.
50. Zhang J, Liang YC, Lin X, et al. Self-monitoring and self-delivery of photosensitizer-doped nanoparticles for highly effective combination cancer therapy in vitro and in vivo. *ACS Nano.* 2015; 9: 9741-56.
51. Cui L, Lin Q, Jin CS, et al. A PEGylation-free biomimetic porphyrin nanoplatform for personalized cancer theranostics. *ACS Nano.* 2015; 9: 4484-95.
52. Rensen PC, de Vruhe RL, Kuiper J, et al. Recombinant lipoproteins: lipoprotein-like lipid particles for drug targeting. *Adv Drug Deliv Rev.* 2001; 47: 251-76.
53. Geim AK, Novoselov KS. The rise of graphene. *Nat Mater.* 2007; 6: 183-91.
54. Yan X, Niu G, Lin J, et al. Enhanced fluorescence imaging guided photodynamic therapy of sinoporphyrin sodium loaded graphene oxide. *Biomaterials.* 2015; 42: 94-102.
55. Choi Y, Kim S, Choi MH, et al. Highly biocompatible carbon nanodots for simultaneous bioimaging and targeted photodynamic therapy in vitro and in vivo. *Adv Funct Mater.* 2014; 24: 5781-89.
56. Huang P, Lin J, Wang S, et al. Photosensitizer-conjugated silica-coated gold nanoclusters for fluorescence imaging-guided photodynamic therapy. *Biomaterials.* 2013; 34: 4643-54.
57. Xie J, Zheng Y, Ying JY. Protein-directed synthesis of highly fluorescent gold nanoclusters. *J Am Chem Soc.* 2009; 131: 888-9.
58. Li Z, Wang C, Cheng L, et al. PEG-functionalized iron oxide nanoclusters loaded with chlorin e6 for targeted, NIR light induced, photodynamic therapy. *Biomaterials.* 2013; 34: 9160-70.
59. Xuan SH, Lee SF, Lau JT, et al. Photocytotoxicity and magnetic relaxivity responses of dual-porous gamma-Fe2O3@meso-SiO2 microspheres. *ACS Appl Mater Interfaces.* 2012; 4: 2033-40.
60. Ling D, Park W, Park SJ, et al. Multifunctional tumor pH-sensitive self-assembled nanoparticles for bimodal imaging and treatment of resistant heterogeneous tumors. *J Am Chem Soc.* 2014; 136: 5647-55.
61. Il Park Y, Lee KT, Suh YD, et al. Upconverting nanoparticles: a versatile platform for wide-field two-photon microscopy and multi-modal in vivo imaging. *Chem Soc Rev.* 2015; 44: 1302-17.
62. Liu K, Liu X, Zeng Q, et al. Covalently assembled NIR nanoplatform for simultaneous fluorescence imaging and photodynamic therapy of cancer cells. *ACS Nano.* 2012; 6: 4054-62.
63. Wang C, Tao H, Cheng L, et al. Near-infrared light induced in vivo photodynamic therapy of cancer based on upconversion nanoparticles. *Biomaterials.* 2011; 32: 6145-54.
64. Idris NM, Gnanasamandhan MK, Zhang J, et al. In vivo photodynamic therapy using upconversion nanoparticles as remote-controlled nanotransducers. *Nat Med.* 2012; 18: 1580-5.
65. Wang C, Cheng L, Liu YM, et al. Imaging-guided pH-sensitive photodynamic therapy using charge reversible upconversion nanoparticles under near-infrared light. *Adv Funct Mater.* 2013; 23: 3077-86.
66. Cui S, Yin D, Chen Y, et al. In vivo targeted deep-tissue photodynamic therapy based on near-infrared light triggered upconversion nanoconstruct. *ACS Nano.* 2013; 7: 676-88.
67. Ai X, Ho CJ, Aw J, et al. In vivo covalent cross-linking of photon-converted rare-earth nanostructures for tumour localization and theranostics. *Nat Commun.* 2016; 7: 10432.
68. Park YI, Kim HM, Kim JH, et al. Theranostic probe based on lanthanide-doped nanoparticles for simultaneous in vivo dual-modal imaging and photodynamic therapy. *Adv Mater.* 2012; 24: 5755-61.
69. Fan W, Shen B, Bu W, et al. A smart upconversion-based mesoporous silica nanotheranostic system for synergetic chemo-/radio-/photodynamic therapy and simultaneous MR/UCL imaging. *Biomaterials.* 2014; 35: 8992-9002.
70. Tian G, Ren W, Yan L, et al. Red-emitting upconverting nanoparticles for photodynamic therapy in cancer cells under near-infrared excitation. *Small.* 2013; 9: 1929-38.
71. Huang P, Lin J, Wang X, et al. Light-triggered theranostics based on photosensitizer-conjugated carbon dots for simultaneous enhanced-fluorescence imaging and photodynamic therapy. *Adv Mater.* 2012; 24: 5104-10.
72. Roberts WG, Smith KM, Mccullough JL, et al. Skin photosensitivity and photodestruction of several potential photodynamic sensitizers. *Photochem Photobiol.* 1989; 49: 431-38.
73. Harris AL. Hypoxia—a key regulatory factor in tumour growth. *Nat Rev Cancer.* 2002; 2: 38-47.
74. Luo SL, Zhang EL, Su YP, et al. A review of NIR dyes in cancer targeting and imaging. *Biomaterials.* 2011; 32: 7127-38.
75. Yu J, Javier D, Yaseen MA, et al. Self-assembly synthesis, tumor cell targeting, and photothermal capabilities of antibody-coated indocyanine green nanocapsules. *J Am Chem Soc.* 2010; 132: 1929-38.
76. Yue C, Liu P, Zheng M, et al. IR-780 dye loaded tumor targeting theranostic nanoparticles for NIR imaging and photothermal therapy. *Biomaterials.* 2013; 34: 6853-61.
77. Huang P, Gao Y, Lin J, et al. Tumor-specific formation of enzyme-instructed supramolecular self-assemblies as cancer theranostics. *ACS Nano.* 2015; 9: 9517-27.
78. Sheng Z, Hu D, Zheng M, et al. Smart human serum albumin-indocyanine green nanoparticles generated by programmed assembly for dual-modal imaging-guided cancer synergistic phototherapy. *ACS Nano.* 2014; 8: 12310-22.
79. Wu L, Fang S, Shi S, et al. Hybrid polypeptide micelles loading indocyanine green for tumor imaging and photothermal effect study. *Biomacromolecules.* 2013; 14: 3027-33.
80. Chen Q, Liang C, Wang X, et al. An albumin-based theranostic nano-agent for dual-modal imaging guided photothermal therapy to inhibit lymphatic metastasis of cancer post surgery. *Biomaterials.* 2014; 35: 9355-62.
81. Huang P, Rong P, Jin A, et al. Dye-loaded ferritin nanocages for multimodal imaging and photothermal therapy. *Adv Mater.* 2014; 26: 6401-8.
82. Chen Q, Liang C, Wang C, et al. An imagable and photothermal "Abraxane-like" nanodrug for combination cancer therapy to treat subcutaneous and metastatic breast tumors. *Adv Mater.* 2015; 27: 903-10.
83. Rong P, Huang P, Liu Z, et al. Protein-based photothermal theranostics for imaging-guided cancer therapy. *Nanoscale.* 2015; 7: 16330-6.
84. Wang Y, Yang T, Ke H, et al. Smart albumin-biomimetic nanocomposites for multimodal imaging and photothermal tumor ablation. *Adv Mater.* 2015; 27: 3874-82.
85. Zheng M, Yue C, Ma Y, et al. Single-step assembly of DOX/ICG loaded lipid-polymer nanoparticles for highly effective chemo-photothermal combination therapy. *ACS Nano.* 2013; 7: 2056-67.
86. Wan Z, Mao H, Guo M, et al. Highly efficient hierarchical micelles integrating photothermal therapy and singlet oxygen-synergized chemotherapy for cancer eradication. *Theranostics.* 2014; 4: 399-411.
87. He XY, Bao XY, Cao HQ, et al. Tumor-penetrating nanotherapeutics loading a near-infrared probe inhibit growth and metastasis of breast cancer. *Adv Funct Mater.* 2015; 25: 2831-39.
88. Peng CL, Shih YH, Lee PC, et al. Multimodal image-guided photothermal therapy mediated by 188Re-labeled micelles containing a cyanine-type photosensitizer. *ACS Nano.* 2011; 5: 5594-607.
89. Zhu A, Miao K, Deng Y, et al. Dually pH/reduction-responsive vesicles for ultrahigh-contrast fluorescence imaging and thermo-chemotherapy-synergized tumor ablation. *ACS Nano.* 2015; 9: 7874-85.
90. Chen Q, Wang C, Cheng L, et al. Protein modified upconversion nanoparticles for imaging-guided combined photothermal and photodynamic therapy. *Biomaterials.* 2014; 35: 2915-23.
91. Ma Y, Tong S, Bao G, et al. Indocyanine green loaded SPIO nanoparticles with phospholipid-PEG coating for dual-modal imaging and photothermal therapy. *Biomaterials.* 2013; 34: 7706-14.
92. He XM, Carter DC. Atomic-structure and chemistry of human serum-albumin. *Nature.* 1992; 358: 209-15.
93. Elzoghby AO, Samy WM, Elgindy NA. Albumin-based nanoparticles as potential controlled release drug delivery systems. *J Control Release.* 2012; 157: 168-82.
94. Munro HN, Linder MC. Ferritin: structure, biosynthesis, and role in iron metabolism. *Physiol Rev.* 1978; 58: 317-96.
95. Yu HJ, Cui ZR, Yu PC, et al. pH- and NIR light-responsive micelles with hyperthermia-triggered tumor penetration and cytoplasm drug release to reverse doxorubicin resistance in breast cancer. *Adv Funct Mater.* 2015; 25: 2489-500.
96. Ding D, Li K, Liu B, et al. Bioprobes based on AIE fluorogens. *Acc Chem Res.* 2013; 46: 2441-53.
97. Yuan Y, Feng G, Qin W, et al. Targeted and image-guided photodynamic cancer therapy based on organic nanoparticles with aggregation-induced emission characteristics. *Chem Commun (Camb).* 2014; 50: 8757-60.
98. Hong Y, Lam JW, Tang BZ. Aggregation-induced emission: phenomenon, mechanism and applications. *Chem Commun (Camb).* 2009: 4332-53.
99. Yuan Y, Zhang CJ, Gao M, et al. Specific light-up bioprobe with aggregation-induced emission and activatable photoactivity for the targeted and image-guided photodynamic ablation of cancer cells. *Angew Chem Int Ed Engl.* 2015; 54: 1780-6.
100. Kim J, Lee E, Hong Y, et al. Self-doped conjugated polymeric nanoassembly by simplified process for optical cancer theragnosis. *Adv Funct Mater.* 2015; 25: 2260-69.
101. Wang C, Xu H, Liang C, et al. Iron oxide @ polypyrrole nanoparticles as a multifunctional drug carrier for remotely controlled cancer therapy with synergistic antitumor effect. *ACS Nano.* 2013; 7: 6782-95.

102. Song XJ, Gong H, Yin SN, et al. Ultra- small iron oxide doped polypyrrole nanoparticles for in vivo multimodal imaging guided photothermal therapy. *Adv Funct Mater.* 2014; 24: 1194-201.
103. Liang XL, Li YY, Li XD, et al. PEGylated polypyrrole nanoparticles conjugating gadolinium chelates for dual-modal MRI/photoacoustic imaging guided photothermal therapy of cancer. *Adv Funct Mater.* 2015; 25: 1451-62.
104. Liu F, He X, Chen H, et al. Gram-scale synthesis of coordination polymer nanodots with renal clearance properties for cancer theranostic applications. *Nat Commun.* 2015; 6: 8003.
105. Cai XJ, Jia XQ, Gao W, et al. A versatile nanotheranostic agent for efficient dual-mode imaging guided synergistic chemo-thermal tumor therapy. *Adv Funct Mater.* 2015; 25: 2520-29.
106. Huang HC, Barua S, Sharma G, et al. Inorganic nanoparticles for cancer imaging and therapy. *J Control Release.* 2011; 155: 344-57.
107. Michalet X, Pinaud FF, Bentolila LA, et al. Quantum dots for live cells, in vivo imaging, and diagnostics. *Science.* 2005; 307: 538-44.
108. Zhao YX, Pan HC, Lou YB, et al. Plasmonic Cu₂-xS nanocrystals: optical and structural properties of copper-deficient copper(I) sulfides. *J Am Chem Soc.* 2009; 131: 4253-61.
109. Goel S, Chen F, Cai WB. Synthesis and biomedical applications of copper sulfide nanoparticles: from sensors to theranostics. *Small.* 2014; 10: 631-45.
110. Park SH, Roy A, Beaupre S, et al. Bulk heterojunction solar cells with internal quantum efficiency approaching 100%. *Nat Photonics.* 2009; 3: 297-U5.
111. Kataura H, Kumazawa Y, Maniwa Y, et al. Optical properties of single-wall carbon nanotubes. *Synth Met.* 1999; 103: 2555-58.
112. Bonaccorso F, Sun Z, Hasan T, et al. Graphene photonics and optoelectronics. *Nat Photonics.* 2010; 4: 611-22.
113. Jin Y, Jia C, Huang SW, et al. Multifunctional nanoparticles as coupled contrast agents. *Nat Commun.* 2010; 1: 41.
114. Li W, Chen X. Gold nanoparticles for photoacoustic imaging. *Nanomedicine (Lond).* 2015; 10: 299-320.
115. Idris NM, Lucky SS, Li ZQ, et al. Photoactivation of core-shell titania coated upconversion nanoparticles and their effect on cell death. *J Mat Chem B.* 2014; 2: 7017-26.
116. Zhang Z, Wang L, Wang J, et al. Mesoporous silica-coated gold nanorods as a light-mediated multifunctional theranostic platform for cancer treatment. *Adv Mater.* 2012; 24: 1418-23.
117. Chen J, Glaus C, Laforest R, et al. Gold nanocages as photothermal transducers for cancer treatment. *Small.* 2010; 6: 811-7.
118. Kuo WS, Chang CN, Chang YT, et al. Gold nanorods in photodynamic therapy, as hyperthermia agents, and in near-infrared optical imaging. *Angew Chem Int Ed Engl.* 2010; 49: 2711-5.
119. Xia Y, Li W, Cobley CM, et al. Gold nanocages: from synthesis to theranostic applications. *Acc Chem Res.* 2011; 44: 914-24.
120. Zhang Z, Wang J, Chen C. Gold nanorods based platforms for light-mediated theranostics. *Theranostics.* 2013; 3: 223-38.
121. Westcott SL, Oldenburg SJ, Lee TR, et al. Construction of simple gold nanoparticle aggregates with controlled plasmon-plasmon interactions. *Chem Phys Lett.* 1999; 300: 651-55.
122. Lu W, Melancon MP, Xiong C, et al. Effects of photoacoustic imaging and photothermal ablation therapy mediated by targeted hollow gold nanospheres in an orthotopic mouse xenograft model of glioma. *Cancer Res.* 2011; 71: 6116-21.
123. Ye SJ, Marston G, McLaughlan JR, et al. Engineering gold nanotubes with controlled length and near-infrared absorption for theranostic applications. *Adv Funct Mater.* 2015; 25: 2117-27.
124. Hembury M, Chiappini C, Bertazzo S, et al. Gold-silica quantum rattles for multimodal imaging and therapy. *Proc Natl Acad Sci U S A.* 2015; 112: 1959-64.
125. Huang P, Rong PF, Lin J, et al. Triphase interface synthesis of plasmonic gold bellflowers as near-infrared light mediated acoustic and thermal theranostics. *J Am Chem Soc.* 2014; 136: 8307-13.
126. Wang X, Wang C, Cheng L, et al. Noble metal coated single-walled carbon nanotubes for applications in surface enhanced Raman scattering imaging and photothermal therapy. *J Am Chem Soc.* 2012; 134: 7414-22.
127. Dong W, Li Y, Niu D, et al. Facile synthesis of monodisperse superparamagnetic Fe₃O₄ Core@hybrid@Au shell nanocomposite for bimodal imaging and photothermal therapy. *Adv Mater.* 2011; 23: 5392-7.
128. Ma Y, Liang XL, Tong S, et al. Gold nanoshell nanomicelles for potential magnetic resonance imaging, light-triggered drug release, and photothermal therapy. *Adv Funct Mater.* 2013; 23: 815-22.
129. Li CM, Chen T, Ocoy J, et al. Gold-coated Fe₃O₄ nanoroses with five unique functions for cancer cell targeting, imaging, and therapy. *Adv Funct Mater.* 2014; 24: 1772-80.
130. Wang DW, Zhu XM, Lee SF, et al. Folate-conjugated Fe₃O₄@SiO₂/gold nanorods@mesoporous SiO₂ hybrid nanomaterial: a theranostic agent for magnetic resonance imaging and photothermal therapy. *J Mater Chem B.* 2013; 1: 2934-42.
131. Huang J, Guo M, Ke H, et al. Rational design and synthesis of gamma-Fe₂O₃@Au magnetic gold nanoflowers for efficient cancer theranostics. *Adv Mater.* 2015; 27: 5049-56.
132. Sun X, Huang X, Yan X, et al. Chelator-free (64)Cu-integrated gold nanomaterials for positron emission tomography imaging guided photothermal cancer therapy. *ACS Nano.* 2014; 8: 8438-46.
133. Deng H, Dai F, Ma G, et al. Theranostic gold nanomicelles made from biocompatible comb-like polymers for thermochemotherapy and multifunctional imaging with rapid clearance. *Adv Mater.* 2015; 27: 3645-53.
134. Song J, Zhou J, Duan H. Self-assembled plasmonic vesicles of SERS-encoded amphiphilic gold nanoparticles for cancer cell targeting and traceable intracellular drug delivery. *J Am Chem Soc.* 2012; 134: 13458-69.
135. Lin J, Wang S, Huang P, et al. Photosensitizer-loaded gold vesicles with strong plasmonic coupling effect for imaging-guided photothermal/photodynamic therapy. *ACS Nano.* 2013; 7: 5320-9.
136. Huang P, Lin J, Li W, et al. Biodegradable gold nanovesicles with an ultrastrong plasmonic coupling effect for photoacoustic imaging and photothermal therapy. *Angew Chem Int Ed Engl.* 2013; 52: 13958-64.
137. Song J, Yang X, Jacobson O, et al. Ultrasmall gold nanorod vesicles with enhanced tumor accumulation and fast excretion from the body for cancer therapy. *Adv Mater.* 2015; 27: 4910-7.
138. Song J, Yang X, Jacobson O, et al. Sequential drug release and enhanced photothermal and photoacoustic effect of hybrid reduced graphene oxide-loaded ultrasmall gold nanorod vesicles for cancer therapy. *ACS Nano.* 2015; 9: 9199-209.
139. Song J, Cheng L, Liu A, et al. Plasmonic vesicles of amphiphilic gold nanocrystals: self-assembly and external-stimuli-triggered destruction. *J Am Chem Soc.* 2011; 133: 10760-3.
140. He J, Liu YJ, Babu T, et al. Self-assembly of inorganic nanoparticle vesicles and tubules driven by tethered linear block copolymers. *J Am Chem Soc.* 2012; 134: 11342-45.
141. Haram SK, Mahadeshwar AR, Dixit SG. Synthesis and characterization of copper sulfide nanoparticles in Triton-X 100 water-in-oil microemulsions. *J Phys Chem.* 1996; 100: 5868-73.
142. Li Y, Lu W, Huang Q, et al. Copper sulfide nanoparticles for photothermal ablation of tumor cells. *Nanomedicine (Lond).* 2010; 5: 1161-71.
143. Ku G, Zhou M, Song S, et al. Copper sulfide nanoparticles as a new class of photoacoustic contrast agent for deep tissue imaging at 1064 nm. *ACS Nano.* 2012; 6: 7489-96.
144. Zhou M, Li J, Liang S, et al. CuS nanodots with ultrahigh efficient renal clearance for positron emission tomography imaging and image-guided photothermal therapy. *ACS Nano.* 2015; 9: 7085-96.
145. Zhou M, Zhang R, Huang M, et al. A chelator-free multifunctional [⁶⁴Cu]CuS nanoparticle platform for simultaneous micro-PET/CT imaging and photothermal ablation therapy. *J Am Chem Soc.* 2010; 132: 15351-8.
146. Liu R, Jing L, Peng D, et al. Manganese (II) chelate functionalized copper sulfide nanoparticles for efficient magnetic resonance/photoacoustic dual-modal imaging guided photothermal therapy. *Theranostics.* 2015; 5: 1144-53.
147. Xiao Q, Zheng X, Bu W, et al. A core/satellite multifunctional nanotheranostic for in vivo imaging and tumor eradication by radiation/photothermal synergistic therapy. *J Am Chem Soc.* 2013; 135: 13041-8.
148. Yi X, Yang K, Liang C, et al. Imaging-guided combined photothermal and radiotherapy to treat subcutaneous and metastatic tumors using Iodine-131-doped copper sulfide nanoparticles. *Adv Funct Mater.* 2015; 25: 4689-99.
149. Zhang L, Gao S, Zhang F, et al. Activatable hyaluronic acid nanoparticle as a theranostic agent for optical/photoacoustic image-guided photothermal therapy. *ACS Nano.* 2014; 8: 12250-8.
150. Chen F, Hong H, Goel S, et al. In vivo tumor vasculature targeting of CuS@MSN based theranostic nanomedicine. *ACS Nano.* 2015; 9: 3926-34.
151. Wu ZC, Li WP, Luo CH, et al. Rattle-type Fe₃O₄@CuS developed to conduct magnetically guided photoinduced hyperthermia at first and second NIR biological windows. *Adv Funct Mater.* 2015; 25: 6527-37.
152. Chou SS, Kaehr B, Kim J, et al. Chemically exfoliated MoS₂ as near-infrared photothermal agents. *Angew Chem Int Ed Engl.* 2013; 52: 4160-4.
153. Liu T, Shi S, Liang C, et al. Iron oxide decorated MoS₂ nanosheets with double PEGylation for chelator-free radiolabeling and multimodal imaging guided photothermal therapy. *ACS Nano.* 2015; 9: 950-60.
154. Yin W, Yan L, Yu J, et al. High-throughput synthesis of single-layer MoS₂ nanosheets as a near-infrared photothermal-triggered drug delivery for effective cancer therapy. *ACS Nano.* 2014; 8: 6922-33.
155. Wang S, Li X, Chen Y, et al. A facile one-pot synthesis of a two-dimensional MoS₂/Bi₂S₃ composite theranostic nanosystem for multi-modality tumor imaging and therapy. *Adv Mater.* 2015; 27: 2775-82.
156. Yu J, Yin W, Zheng X, et al. Smart MoS₂/Fe₃O₄ nanotheranostic for magnetically targeted photothermal therapy guided by magnetic resonance/photoacoustic imaging. *Theranostics.* 2015; 5: 931-45.
157. Cheng L, Liu J, Gu X, et al. PEGylated WS₂ nanosheets as a multifunctional theranostic agent for in vivo dual-modal CT/photoacoustic imaging guided photothermal therapy. *Adv Mater.* 2014; 26: 1886-93.
158. Cheng L, Yuan C, Shen S, et al. Bottom-up synthesis of metal-ion-doped WS₂ nanoflakes for cancer theranostics. *ACS Nano.* 2015; 9: 11090-101.
159. Yang G, Gong H, Liu T, et al. Two-dimensional magnetic WS₂@Fe₃O₄ nanocomposite with mesoporous silica coating for drug delivery and imaging-guided therapy of cancer. *Biomaterials.* 2015; 60: 62-71.
160. Qian X, Shen S, Liu T, et al. Two-dimensional TiS₂ nanosheets for in vivo photoacoustic imaging and photothermal cancer therapy. *Nanoscale.* 2015; 7: 6380-7.

161. Yang K, Yang G, Chen L, et al. FeS nanoplates as a multifunctional nano-theranostic for magnetic resonance imaging guided photothermal therapy. *Biomaterials*. 2015; 38: 1-9.
162. Liu J, Zheng X, Yan L, et al. Bismuth sulfide nanorods as a precision nanomedicine for in vivo multimodal imaging-guided photothermal therapy of tumor. *ACS Nano*. 2015; 9: 696-707.
163. Song G, Liang C, Gong H, et al. Core-shell MnSe@Bi₂Se₃ fabricated via a cation exchange method as novel nanotheranostics for multimodal imaging and synergistic theranostic. *Adv Mater*. 2015; 27: 6110-7.
164. Song XR, Wang X, Yu SX, et al. Co₉Se₈ nanoplates as a new theranostic platform for photoacoustic/magnetic resonance dual-modal-imaging-guided chemo-photothermal combination therapy. *Adv Mater*. 2015; 27: 3285-91.
165. Kam NWS, O'Connell M, Wisdom JA, et al. Carbon nanotubes as multifunctional biological transporters and near-infrared agents for selective cancer cell destruction. *Proc Natl Acad Sci U S A*. 2005; 102: 11600-05.
166. Liu Z, Cai W, He L, et al. In vivo biodistribution and highly efficient tumor targeting of carbon nanotubes in mice. *Nat Nanotechnol*. 2007; 2: 47-52.
167. Singh R, Pantarotto D, Lacerda L, et al. Tissue biodistribution and blood clearance rates of intravenously administered carbon nanotube radiotracers. *Proc Natl Acad Sci U S A*. 2006; 103: 3357-62.
168. Liu Z, Davis C, Cai W, et al. Circulation and long-term fate of functionalized, biocompatible single-walled carbon nanotubes in mice probed by Raman spectroscopy. *Proc Natl Acad Sci U S A*. 2008; 105: 1410-5.
169. Moon HK, Lee SH, Choi HC. In vivo near-infrared mediated tumor destruction by photothermal effect of carbon nanotubes. *ACS Nano*. 2009; 3: 3707-13.
170. Antaris AL, Robinson JT, Yaghi OK, et al. Ultra-low doses of chirality sorted (6,5) carbon nanotubes for simultaneous tumor imaging and photothermal therapy. *ACS Nano*. 2013; 7: 3644-52.
171. Liu JJ, Wang C, Wang XJ, et al. Mesoporous silica coated single-walled carbon nanotubes as a multifunctional light-responsive platform for cancer combination therapy. *Adv Funct Mater*. 2015; 25: 384-92.
172. Cao MS, Yang J, Song WL, et al. Ferroferric oxide/multiwalled carbon nanotube vs polyaniline/ferroferric oxide/multiwalled carbon nanotube multiheterostructures for highly effective microwave absorption. *ACS Appl Mater Interfaces*. 2012; 4: 6949-56.
173. Liang C, Diao S, Wang C, et al. Tumor metastasis inhibition by imaging-guided photothermal therapy with single-walled carbon nanotubes. *Adv Mater*. 2014; 26: 5646-52.
174. Yang K, Feng L, Shi X, et al. Nano-graphene in biomedicine: theranostic applications. *Chem Soc Rev*. 2013; 42: 530-47.
175. Yoo JM, Kang JH, Hong BH. Graphene-based nanomaterials for versatile imaging studies. *Chem Soc Rev*. 2015; 44: 4835-52.
176. Yang K, Zhang S, Zhang G, et al. Graphene in mice: ultrahigh in vivo tumor uptake and efficient photothermal therapy. *Nano Lett*. 2010; 10: 3318-23.
177. Robinson JT, Tabakman SM, Liang YY, et al. Ultrasmall reduced graphene oxide with high near-infrared absorbance for photothermal therapy. *J Am Chem Soc*. 2011; 133: 6825-31.
178. Hu SH, Chen YW, Hung WT, et al. Quantum-dot-tagged reduced graphene oxide nanocomposites for bright fluorescence bioimaging and photothermal therapy monitored in situ. *Adv Mater*. 2012; 24: 1748-54.
179. Yang K, Hu L, Ma X, et al. Multimodal imaging guided photothermal therapy using functionalized graphene nanosheets anchored with magnetic nanoparticles. *Adv Mater*. 2012; 24: 1868-72.
180. Shi X, Gong H, Li Y, et al. Graphene-based magnetic plasmonic nanocomposite for dual bioimaging and photothermal therapy. *Biomaterials*. 2013; 34: 4786-93.
181. Ge J, Jia Q, Liu W, et al. Red-emissive carbon dots for fluorescent, photoacoustic, and thermal theranostics in living mice. *Adv Mater*. 2015; 27: 4169-77.
182. Ge J, Lan M, Zhou B, et al. A graphene quantum dot photodynamic therapy agent with high singlet oxygen generation. *Nat Commun*. 2014; 5: 4596.
183. Moon H, Kumar D, Kim H, et al. Amplified photoacoustic performance and enhanced photothermal stability of reduced graphene oxide coated gold nanorods for sensitive photo acoustic imaging. *ACS Nano*. 2015; 9: 2711-19.
184. Ding XG, Liow CH, Zhang MX, et al. Surface plasmon resonance enhanced light absorption and photothermal therapy in the second near-infrared window. *J Am Chem Soc*. 2014; 136: 15684-93.
185. Zhu XL, Shi L, Schmidt MS, et al. Enhanced light-matter interactions in graphene-covered gold nanovoid arrays. *Nano Lett*. 2013; 13: 4690-96.
186. Gong H, Dong ZL, Liu YM, et al. Engineering of multifunctional nano-micelles for combined photothermal and photodynamic therapy under the guidance of multimodal imaging. *Adv Funct Mater*. 2014; 24: 6492-502.
187. Guo M, Mao H, Li Y, et al. Dual imaging-guided photothermal/photodynamic therapy using micelles. *Biomaterials*. 2014; 35: 4656-66.
188. Song X, Liang C, Gong H, et al. Photosensitizer-conjugated albumin-polyproline nanoparticles for imaging-guided in vivo photodynamic/photothermal therapy. *Small*. 2015; 11: 3932-41.
189. Chen R, Wang X, Yao X, et al. Near-IR-triggered photothermal/photodynamic dual-modality therapy system via chitosan hybrid nanospheres. *Biomaterials*. 2013; 34: 8314-22.
190. Jang B, Park JY, Tung CH, et al. Gold nanorod-photosensitizer complex for near-infrared fluorescence imaging and photodynamic/photothermal therapy in vivo. *ACS Nano*. 2011; 5: 1086-94.
191. Wang Y, Wang H, Liu D, et al. Graphene oxide covalently grafted upconversion nanoparticles for combined NIR mediated imaging and photothermal/photodynamic cancer therapy. *Biomaterials*. 2013; 34: 7715-24.
192. Lv R, Yang P, He F, et al. A yolk-like multifunctional platform for multimodal imaging and synergistic therapy triggered by a single near-infrared light. *ACS Nano*. 2015; 9: 1630-47.
193. Henderson TA, Morris LD. Near-infrared photonic energy penetration: can infrared phototherapy effectively reach the human brain? *Neuropsychiatr Dis Treat*. 2015; 11: 2191-208.
194. Cheng L, Wang C, Feng L, et al. Functional nanomaterials for phototherapies of cancer. *Chem Rev*. 2014; 114: 10869-939.
195. Zhen Z, Tang W, Chuang YJ, et al. Tumor vasculature targeted photodynamic therapy for enhanced delivery of nanoparticles. *ACS Nano*. 2014; 8: 6004-13.
196. Hong G, Wu JZ, Robinson JT, et al. Three-dimensional imaging of single nanotube molecule endocytosis on plasmonic substrates. *Nat Commun*. 2012; 3: 700.
197. Wang C, Xu L, Liang C, et al. Immunological responses triggered by photothermal therapy with carbon nanotubes in combination with anti-CTLA-4 therapy to inhibit cancer metastasis. *Adv Mater*. 2014; 26: 8154-62.
198. Song CW. Effect of local hyperthermia on blood flow and microenvironment: a review. *Cancer Res*. 1984; 44: 4721s-30s.
199. Min Y, Caster JM, Eblan MJ, et al. Clinical translation of nanomedicine. *Chem Rev*. 2015; 115: 11147-90.
200. Kolosnjaj-Tabi J, Javed Y, Lartigue L, et al. The one year fate of iron oxide coated gold nanoparticles in mice. *ACS Nano*. 2015; 9: 7925-39.
201. Soenen SJ, Rivera-Gil P, Montenegro JM, et al. Cellular toxicity of inorganic nanoparticles: Common aspects and guidelines for improved nanotoxicity evaluation. *Nano Today*. 2011; 6: 446-65.
202. Helmchen F, Denk W. Deep tissue two-photon microscopy. *Nat Methods*. 2005; 2: 932-40.
203. Bagley AF, Hill S, Rogers GS, et al. Plasmonic photothermal heating of intraperitoneal tumors through the use of an implanted near-infrared source. *ACS Nano*. 2013; 7: 8089-97.